Addis Ababa University

Addis Ababa Institute of Technology

Center of Biomedical Engineering

Slice Based 3D Cell Segmentation of Optical Projection Tomography Images

A thesis submitted to Addis Ababa Institute of Technology, School of Graduate Studies, Addis Ababa university

In partial fulfillment of the requirement for the Degree of Master of Science in Biomedical Engineering

By: Haile Baye Kassahun

Advisors: Birhanu Assefa Belay (PhD Candidate)

Professor Jari Hyttinen

Dr. Dawit Assefa Haile

Addis Ababa, Ethiopia

January, 2018

Certificate of Examination

Addis Ababa University

Addis Ababa Institute of Technology

Center of Biomedical Engineering

Slice Based 3D Cell Segmentation of Optical Projection Tomography Images

By: Haile Baye Kassahun

APPROVED BY BOARD OF EXAMINERS

Chairman, Department of Graduate Committee	Signature
Birhanu Assefa Belay	
Professor Jari Hyttinen	
Dr. Dawit Assefa Haile	
Name of Advisors	Signature
Name of External Examiner	Signature
Name of Internal Examiner	Signature

Acknowledgment

First and foremost I would like to give my best gratitude to my first advisor Birhanu Assefa who gave me a chance to work on this interesting research topic in the first place. And also who advised and guided me throughout the year. Your valuable comments despite your very tight schedule was indeed useful and I am very grateful for that.

Second, I would like to thank my second advisor professor Jari Hyttinen who brought the idea of the thesis and also helped me to go in the right direction. your willingness to send me the datasets on time without any kind of reservations is highly appreciated. And thank you for that.

Third, my heartfelt gratitude goes to my third advisor Dr. Dawit Assefa who guided and advised me through out the year with an incredible devotion. Thank you for your profound and wise insights you provided me. Hadn't it been your kind support, I would not have brought my thesis to this level.

Fourth, my gratitude goes to Janne Koivisto who prepared the 3D gellan gum hydrogel scaffold for imaging.

Fifth, I would like to thank Robel Kebede for his wise advice while I was writing my thesis proposal.

Last but not least, I would like to extend my gratitude to my classmates who provided me useful comments. In addition to this, I would also like to thank my families specially my aunt Yalganesh Dress who dedicates her life for the entire family. And my brother Tewodros who helped me in adjusting the images on photoshop.

Declaration

I declare that this thesis is my work and that all sources of materials used for this thesis have been properly acknowledged. This thesis has been submitted in partial fulfillment of the requirements for M.Sc. degree in Biomedical Engineering at Addis Ababa University. I earnestly declare that this thesis is not submitted to any other institution any where for the award of any academic degree, diploma, or certificate.

Name: Haile Baye Kasshun

Signature:_____

Place: Addis Ababa, Ethiopia

Date of Submission:_____

This thesis has been submitted for our approval as a university advisors.

Name: Birhanu Assefa Belay

Signature:_____

Name: Dr. Dawit Assefa Haile

Signature:_____

Place: Addis Ababa, Ethiopia

Date:_____

Abstract

Optical Projection Tomography (OPT) is a new imaging technique used to image cells in 3D cultured in a hydrogel. Reconstructed OPT images of cells suffer from several artifacts. These artifacts reduce the overall image quality. This will create a challenge for isolating and studying each cell in 3D cell culture. It is highly required to enhance the 3D OPT images of cells for successful analysis of cell interaction and growth in 3D cell culture. In that regard, this thesis intends to build a robust algorithm for use in effective segmentation of cells cultured inside hydrogel. There exist various 3D cell segmentation algorithms in the literature including those schemes that rely on thresholding, edge detection, region growing and clustering approaches. Among these algorithms, moving average adaptive thresholding (MAAT) and region growing algorithm present commendable performance in segmentation of cells identified on OPT images. In this thesis the performance of an automatic seeded region growing algorithm (ASRGA) and MAAT have been compared rigorously in terms of their use in 2D slice based segmentation of the cells on the 3D OPT image sets considered. Results have shown that the MAAT method show superior performance and provide promising 3D visualization of cells. The output of the research will have a tremendous contribution to reduce artifacts in 3D cell images and enhance 3D visualization.

Key words: Optical Projection Tomography, hydrogel, cell segmentation, region growing algorithm, moving average.

Contents

Certificate of Examination i

Acknowledgment ii

Declaration iii

Abstract iv

List of Figures **vii**

List of Tables **ix**

Acronyms **x**

1 Introduction **1**

1.1 Problem Statement 3

1.2 Objective 4

1.2.1 General Objective 4

1.2.2 Specific Objectives 4

1.3 Significance of the Thesis 4

1.4 Thesis Scope and Delimitations 5

1.5 Organization of the Thesis 5

2 Fundamentals of Optical Projection Tomography **6**

2.1 Optical Projection Tomography (OPT) 6

2.2 Image Processing 9

2.2.1 Preprocessing 9

2.2.2 Segmentation 10

3 Effective Analysis of Cells based on OPT Image Processing **16**

3.1 Materials 16

3.2 Image Acquisition 16

3.3 Preprocessing 17

3.4 Segmentation 19
3.4.1 Automatic Seeded Region Growing Algorithm 19
3.4.2 Moving Average Adaptive Thresholding Algorithm 22
3.5 Post Processing 24
3.6 Stacking Segmented Images to 3D 25
3.7 Volume Quantification 26
3.8 Deconvolution of 2D Projection Images 27

4 Results and Discussion **29**
4.1 Preprocessing 29
4.2 Segmentation 33
4.2.1 Simple Thresholding 33
4.2.2 Automatic Seeded Region Growing Algorithm 34
4.2.3 Moving Average Adaptive Thresholding Technique 35
4.3 Post Processing of Cell Slice Images 38
4.4 Slice Based Cell Counting and Cell Area Calculation 40
4.5 3D Stacking and Analysis Using MATLAB 42
4.5.1 Volume Quantification in Matlab 43
4.6 3D Stacking and Analysis using ImageJ 44
4.7 3D Volume Qauntification using ImageJ 49
4.8 Comparison of MAAT and ASRG Algorithms 50
4.9 Result of Deconvolution of Projection Images Using PSF 51

5 Conclusion and Recommendation **54**
5.1 Conclusion 54
5.2 Recommendation 55

Bibliography **56**

List of Figures

3.1 Samples inserted in FEP tubes are rotated in the rotation stage (S) inside an index matching water bath (B). A white light (LED 1) and a telecentric lens (L) are used for bright-field imaging in transmission OPT mode. Fluorescence illumination is done with 470 nm wavelength LED (LED 2), a band pass filter (F) and collimated with a lens with diffuser (LD) in emission OPT mode. The detection system consists of objective lens (Ob), a rotating filter wheel (FW) filter for a band-pass filter (used only for fluorescence imaging), a pinhole (P), a tube lens (TL), and a sCMOS camera [15]. 17

3.2 Flow chart of the proposed seed selection algorithm. 21

3.3 Flow chart of region growing algorithm. 22

3.4 Block diagram of the proposed scheme. 26

4.1 (a) Original cell slice image, and (b) Automatically cropped image. 29

4.2 Typical histogram of cell slice images. 30

4.3 (a) Original cropped image, and (b) Image after removal of ring-like tube walls. 31

4.4 (a) Original cropped image, and (b) Filtered image using adaptive wiener filter. 32

4.5 (a) Preprocessed image, and (b) Segmented slice image using simple thresholding. 33

4.6 (a) Preprocessed image, (b) Segmented slice image using simple thresholding algorithm, and (c) Segmented slice image using ASRG. 35

4.7 (a) Preprocessed image of slice 1, (b) Preprocessed image of slice 2, (c) Segmented image of slice 1 using ASRG, (d) Segmented image of slice 2 using ASRG , (e) Segmented image of slice 1 using MAAT, and (f) Segmented image of slice 2 using MAAT. 37

4.8 Image subtraction result of moving average adaptive thresholding and automatic seeded region growing algorithm (region growing-moving average). . . 38

4.9 Post processing result: (a) Original cropped image, (b) Preprocessed image, (c) Segmented image using moving average, and (d) Postprocessed image. . 40
4.10 Matlab based area calculation: (a) Segmented slice of automatic seeded region growing for area calculation, and (b) Segmented slice of moving average adaptive thresholding for area calculation. 41
4.11 Matlab 3D stacking results: 3D stacking of 150 segmented cell image slices top view (a) and side view (b). 43
4.12 3D labeled cells for volume quantification 44
4.13 ImageJ 3D stacking results: (a) 3D stacking of 500 segmented cell image slices top view (a) and side view (b). 45
4.14 ImageJ based 3D top view visualization of OPT segmented cell image volume using automatic seeded region growing algorithm (a) and moving average adaptive thresholding method (b). 47
4.15 ImageJ based 3D side view visualization of OPT segmented cell image volume using automatic seeded region growing algorithm (a) and moving average adaptive thresholding method (b). 48
4.16 Cell Labeling applied on the first OPT cell image slice. 49
4.17 The shape of the calculated PSF. 52
4.18 Deconvolution result: (a) Original projection image, (b) Deconvolved projection image using the calculated PSF after 10 iterations, and (c) Deconvolved projection image using the calculated PSF after 400 iterations. 53

List of Tables

4.1 Relationship between average noise/cell and local window of adaptive wiener noise removal filter. 32

4.2 Cell numbers and their corresponding area in pixels matlab result for moving average adaptive thresholding and automatic seeded region growing algorithm. 42

4.3 3D Cell numbers and their corresponding volume Matlab result (2D segmentation algorithm: MAAT). 44

4.4 Statistics of first cell. 50

4.5 Volume of the first 5 labeled cells in Figure 4.16 in cubic micrometer using ASRG and MAAT algorithms. 50

4.6 Comparison of the performance of the two algorithms namely automatic seeded region growing and moving average adaptive thresholding. 51

Acronyms

ASRGA	Automatic Seeded Region Growing Algorithm
AWA	Adaptive Weighting Averaging
CCD	Charge Coupled Device
DOF	Depth Of Field
FBP	Filtered Back Projection
FLIM	Flourescence Lifetime Imaging
MAAT	Moving Average Adaptive Thresholding
MTF	Modulation Transfer Function
OPT	Optical Projection Tomography
PSF	Point Spread Function
sCMOS	scientific Complementary Metal Oxide Semiconductor
ROI	Region Of Interest

Chapter 1

Introduction

Optical Projection Tomography (OPT) is non-invasive, non-destructive and high-resolution 3D optical imaging technique [1][2]. It is suitable for imaging samples in the range of 1-10 mm in diameter [2]. OPT can be used to image both fluorescent and non fluorescent biological specimens [3].

OPT is the optical equivalent of X-ray micro computed tomography (X-ray μCT) [3]. Like μCT, OPT uses filtered back projection technique to reconstruct the images. However, OPT uses photons in the visible spectrum range as opposed to μCT which uses photons in the X-ray spectrum. The use of photons in visible spectrum in optical systems including OPT results in finite depth of field. Moreover, filtered back projection technique in μCT assumes parallel lights as the deflection of X-ray photons is very small. In OPT, however, the straight ray approximation of filtered back projection ignores the diffraction of light by the focusing lens [4]. This will in turn have a blurring effect in both tangential and radial directions of the final reconstructed image [4]. Moreover, there are other artifacts in OPT images. For instance smear artifacts are created due to illumination intensity fluctuation during reconstruction of images [5]. Bowl artifacts are also resulted from reconstruction of truncated projections [5]. Spherical aberration of lenses could also be an other source of artifacts because when light waves pass through the center and periphery of the lens, they won't focus on the same point and this leads to poor resolution in the final image. Moreover, there are also line artifacts which are caused by high intensity spikes ('hot pixels') due to the nature of the detectors. Unique detector edge artifacts are also caused due to nonzero background signal [5]. These combined artifacts result in poor quality of images in OPT which in turn result in poor 3D visualization of cells.

Several approaches have been used in the literature to reduce these OPT image artifacts.

For instance, Walls et al. [5] were able to minimize different noises such as read noise, dark current and pattern noise which are usually created by detection problems on the charge coupled device (CCD). To do this, they calibrated the instrument properly prior to commencing detection of slices [5]. In an other study in order to reduce hot pixels (high intensity pixels) on the reconstructed image, a study by Birk et al. utilized the median filter applied over a 9×9 translating window and the approach decreased the artifacts significantly [6].

More recently the Full Modulation Transfer Function (MTF) was included as additional filter in filtered back projection. It reduces some of the artifacts. However, it does not fully reduce the tangential blurring observed in the image [8]. The work by Horst and Kalkman used image deconvolution technique on sample images of flourescent beads and zebrafish to get the deblurred reconstructed image [8]. They applied the debluring right after the image is converted from frequency domain to spatial domain using the inverse radon transform. They did the deblurring in cylindrical coordinate and convert it back to rectangular coordinate system. This helps to reduce blurrings of OPT images. Nevertheless, the inter conversion from one coordinate system to other takes several minutes to process on a standard desktop computer.

This thesis intends to develop a robust technique applied to OPT images for effective enhancement of image quality and reduction of artifacts in order to efficiently analyze cells identified on 3D cell culture. The technique adheres to two important image processing steps: preprocessing and effective segmentation of cells. Image spikes, circular patterns around periphery of images and similar other artifacts are considered to be addressed during the preprocessing stage. The segmentation is fundamentally 2D, slice based which can be visualized using volume rendering. Focus is given to region growing and adaptive thresholding with their merits and demerits. Performance of the preprocessing as well as segmentation steps are evaluated rigorously both in 2D and 3D.

1.1 Problem Statement

3D cell images of OPT are vulnerable to several artifacts. As a result, it is highly required to enhance 3D cell images which in turn help to study cell differentiation, cell growth and cell migration (motion). Since cellular morphology is an important phenotypic feature and cell contours are required for analysis for the intracellular process, the issue of cell segmentation has received increasing attention in the past years [9]. However, if the image of the cells is not properly processed, it will be difficult to study the aforementioned cell to cell interactions appropriately, which might lead to wrong interpretations. So accurate segmentation of OPT images is required to understand different cell interactions. In this regard, different researchers came up with varieties of algorithms that do microscopic cellular image segmentation. Some of the algorithms such as simple thresholding method mainly depend on the intensity difference of the cell and the background and have low accuracy unless they are combined with other techniques or are made smart enough to adapt to different images. This thesis intends to develop an efficient scheme for segmentation of OPT images based on moving average adaptive thresholding (MAAT) and automatic seeded region growing (ASRG) algorithms proceeded by an effective preprocessing stage.

1.2 Objective

1.2.1 General Objective

- To segment and enhance 3D cell visualization of OPT images using image processing techniques.

1.2.2 Specific Objectives

- To do automatic preprocessing of OPT cell images for reducing artifacts.
- To apply and test different algorithms such as automatic seeded region growing (ASRG) algorithm and moving average adaptive thresholding (MAAT) algorithm for segmenting slice images of the cells.
- To do post-processing of segmented images using dilation operators such as closing and opening operators.
- To stack the segmented slice images to 3D image using Matlab and imageJ softwares.
- To quantify the cells i.e. calculate 3D volume of cells.
- To enhance OPT projection images using Point Spread Function (PSF) based deconvolution technique.

1.3 Significance of the Thesis

It is well known that there are several artifacts generated during image acquisition and reconstruction steps of OPT imaging systems. And this makes the study of cells in 3D cell culture more challenging. The thesis aims to reduce varieties of artifacts that occur in OPT images using image processing techniques. Moreover, the slice based segmentation and 3D stacking in Matlab and ImageJ will greatly enhance the visualization of cells in 3D. Also among other potential clinical implications, accurate quantification of cells

should help biologists and tissue engineers to study cell interactions easily during cell development.

1.4 Thesis Scope and Delimitations

The thesis incorporates 2D slice based preprocessing, segmentation and postprocessing as well as 3D stacking and visualization of OPT images using Matlab and ImageJ platforms. Quntification of OPT cells in 3D is also with in the scope of the thesis. In addition, PSF based deconvolution technique is applied to enhance 2D projection images of OPT. Topics including cell segmentations in 3D space and clinical evaluation of the developed image processing scheme are not considered.

1.5 Organization of the Thesis

The rest of the thesis is organized into four chapters. Chapter 2 deals with various reviewed literatures on topics of OPT and image segmentation techniques. Chapter 3 mainly deals with two segmentation schemes which are applied to segment the cell slice images and 3D stacking methods of the slices for 3D visualization. Chapter 4 presents important results found in this study with discussions while conclusion and future directions are included in the last chapter.

Chapter 2

Fundamentals of Optical Projection Tomography

2.1 Optical Projection Tomography (OPT)

There have been different researches done previously on OPT images. OPT is a relatively new imaging technology with cellular level resolution [3][5]. OPT can be divided into two types: emission OPT and transmission OPT. Emission OPT is when a wide field illumination light strikes on the flourophores and the light emitted from the fluorophore is collected to create an image, whereas transmission OPT is when the source light passes through the specimen and the transmitted light will be collected to create an image.

Fundamentally, tomographic images deals with reconstructing cross sectional images from their projections [2]. In OPT, the 3D structure (stack of x-y slices) of a rotating sample is reconstructed from a series of wide field (2D projections) (x-z images). And the reconstructed slices are stacked into 3D to visualize the sample in 3D.

OPT has various applications. OPT can be applied to image samples that have sizes in the range of 1-10 mm scales [2]. It has a number of applications on fixed specimens which have been made transparent by chemical staining [10]. For instance, it has been applied to image adult mouse organs [10]. OPT can also be applied for gene expression study [11]. It is used to study RNA and protein expression and this helps to understand biological functions and interactions of genes in developmental biology [11]. OPT has important applications for morphology and histopathology researches as well especially in the growing field of mouse model of disease [2]. For example, OPT allows accurate localization and measurement of beta cells in type 2 diabetic disease [2]. As OPT is nondestructive and possess good imaging depth, it can be used to characterize hydrated hydrogels without the need of sample processing [12]. OPT can also be conveniently applied to study plant

growth in 3D [13]. For instance, OPT was applied to visualize variety of plant materials at range of scales including seedlings, leaves, flowers and growing plant tissue such as meristems [13]. OPT can also be extended to FLIM-OPT, a combination of Fluorescence Lifetime Imaging (FLIM) and OPT which is useful for measuring 3D life time information and investigation of 3D biological processes such as for visualizing apoptosis in live Zebrafish larvae [14]. OPT technique can also be used to do imaging experiments and analysis of 3D cultures of cells [3]. For example, it can be used for analysis of beating aggregates of muscular tissue cells in heart [3].

In a recent study, Belay et al. [15] applied OPT to image cells in 3D hydrogel cell culture for the first time. Since OPT is non-invasive, non-toxic and high resolution imaging technique, it was found to be convenient to image cells in 3D as compared to other imaging modalities such as multiphoton microsecope and X-ray based μCT [15]. The bright field cell slice images obtained by OPT were used to test and evaluate the performance of the segmentation algorithm developed in this thesis work.

In OPT, a sample in an index matching liquid is rotated and a projection is acquired at each angular position [1]. Then, standard reconstruction algorithms such as filtered back projection (FBP) are used to reconstruct each projection images to 3D volume [15]. Back projection technique is a way of simply running the projection back through the image to obtain rough approximation to the original sample. It is usually apparent to see blurring in some part of the reconstructed images. This is because the low frequency signals are sampled much more than the high frequency signals. Therefore, high pass filtering is required to eliminate the blurring. Ramp filter is usually used to eliminate such kind of blurring. The combination of back projection and ramp filter is known as filtered back projection (FBP). Generally the complete FBP process which is applied in OPT can be divided into four steps. These are: Fourier transform of measured projection data, multiplication by weighting factor (i.e as convolution in spatial domain is equivalent to multiplication in frequency domain), inverse Fourier transform and summation over the

image plane (the back projection process). The back projection process can be visualized as smearing of each filtered projection over the entire image plane. The standard FBP in an OPT is used with parallel beam projection data [2].

Infact FBP has good accuracy in CT image reconstruction. Nevertheless, when we apply FBP for acquiring OPT images, there are challenges such as image degradation due to refractive index mismatch, light scattering as well as tangential and radial blurring of the 3D reconstruction due to mechanical instability of the instrument which might affect the quality of the images generated [6]. Moreover, FBP assumes parallel ray approximation, it ignores diffraction by the focusing lenses. Using FBP and applying high numerical aperture lens improve the resolution of the optical projection images. Nevertheless, it will have limited depth of field and we won't be able to see the whole sample with depth [4]. Deconvolution techniques after FBP reconstruction are also used to improve the images however such a step has a disadvantage of amplifying noise unless it is done with correct PSF [4].

Generally, poor reconstruction technique and other artifacts combined together result in poor quality of images in OPT. In this regard, there are several techniques proposed in the literature to minimize the OPT image artifacts. One of these techniques is improving the reconstruction strategy. Trull et al. [4] applied a PSF based reconstruction technique on emission OPT images of fluorescent beads and zebrafish larva. They first calculated the PSF of the system. And then discritized the PSF and the image. Next, they multiplied the modulation transfer function (Fourier transform of the PSF) with the fourier transform of the image to be reconstructed. Finally, they applied least square optimization technique to minimize the error between the output image and the product image. They used several iterations to get a good output image. Their iterative reconstruction technique resulted in improved images as compared to those of the standard FBP results.

The other method is the idea of reducing the artifacts of FBP reconstructed images using

image processing techniques. Applying different preprocessing algorithms in spatial or frequency domain can help to reduce blurring and several other types of artifacts. And then to enhance certain region of interest (ROI) of the image, variety of medical image segmentation algorithms might be applied. Medical image segmentation algorithms are usually applied for enhancing medical images for diagnosis and therapeutic purposes. These algorithms can also be used to enhance cell images for analyzing and studying of cell development in 3D cell culture.

2.2 Image Processing

2.2.1 Preprocessing

Preprocessing of cell images is an important step in image processing. It means a way of making the image convenient for processing and post processing stages. Batenberg et al. [16] used a homomorphic processing to compensate unevenness in lighting during the preprocessing stage of bacterial microscopy image segmentation. Moreover, they used Vincent Dome Transform and median filtering for denoising the images. In thier work, median filter was used to remove salt and paper noises.

Jin et al. [17] used adaptive weighting averaging (AWA) technique to estimate the second order statistics such as local mean and variance required by the wiener filter. They first calculated the weighting factor of the mean and the variance, then they estimated the mean and variance of the wiener filter based on the weighting factors. This denoising technique had better accuracy as compared to non-weighted adaptive wiener filter. Nevertheless, the method was unable to remove the dot like noises in the cell images effectively. Therefore, the authors tried wavelet based denoising filters. Even if the weighted wavelet based filters offered more accurate results than the traditional wavelet based ones, they were not effective in removing ripple like artifacts. As a result, the authors applied a combination of weighted spatial based wiener filter and wavelet based filter and they got

improved results.

Strella [18] has applied Wiener filter to blocks of wavelet coefficients. The study followed steps below: first an orthogonal wavelet decomposition of an image corrupted by the gaussian white noise is performed. Then general block covariance and the covariance matrix of each block were estimated. Finally a wiener filter was applied to each block. Following these procedures, the author was able to get good results as compared to the wiener2 filter built in Matlab.

Median filters are often used to remove impulsive noises or salt and pepper type of noises. These filters are better than the mean filters in preserving useful information in the image. Wiener filter is usually used to remove additive gaussian noises. Nagu et al. [19] cascaded median and wiener filters in series and found good results in denoising noise degraded images.

2.2.2 Segmentation

Image segmentation is an important process that separates objects from background and also from each other. The advent of con-focal microscope systems in 1980s opened the door for three dimensional (3D) cell image analysis using segmentation techniques. Cell image analyses have been the basis for numerous studies such as cell counting (numbers), identification of cell types (phases), the quantification of cell migration (morph dynamics), cellular sociology (tissue level organization) and intracellular structure (cell organization) [9]. There are several methods which are applied for cell segmentations. These include:

- Variational Methods (contour based segmentations)
- Intensity Based Thresholding
- Edge Detection Based Segmentation
- Bottle Neck Detection and Ellipse Fitting Segmentation

- Segmentation Based on Clustering
- Region Based Segmentation Methods

Even if there are varities of image segementation methods, selection of an appropriate segmentation technique depends on type of image and applications [20].

Variational Methods (Contour Based Segmentations)

Variational method image segmentation techniques are based upon an energy functional (function of function) where the optimum function represents a good segmentation. The functional depends on a curve parameter. Contour based algorithms such as snakes are parts of variational methods. The major drawback of these algorithms is the fact that the functional is highly dependent on the curve parameterization. Hence the curve parameterization determine the partitioning of the image and terms such as image intensity and image gradient, The variation of the curve parameter will indirectly affect the segmentation result. As a result when the curve parametrization changes, the functional energy will also change and the change of the functional energy is something undesirable because it will affect the image segmentation result [21].

Intensity Based Thresholding

Intensity based thresholding method assumes that the intensity of the cells is quite different from the background signal and segments the cells. This technique may work fine for images having a high contrast between the object and the background. It is specially suitable for images that have bimodal histograms, i.e. if the histogram of the image has a valley and a peak, global thresholding may be applied to differentiate the object and the background easily [22]. But it is a poor segmentation technique for specially low contrast images unless it is combined with other segmentation techniques or unless it is smartly made adaptive. There are pitfalls of thresholding techniques if the optimum global thresholding value is not found. Some of them include smaller or larger segmented regions and

edges of segmented regions might not be connected. However, adaptive thresholding which selects the thresholding value based on the statistical properties (mean, variance and standard deviation) of the images and multi-thresholding which segments medical cell images based on multiple thresholding values often have better accuracy.

Edge Detection Based Segmentation

Edge detection based segmentation techniques are usually applied for images that have intensity discontinuities and borders. They are usually either search based methods or zero crossing methods. The search based methods detect positions and directions using the gradient magnitude, i.e. by applying first order derivatives on the image, whereas the zero crossing methods find the position and direction of edges using laplacian operators. The main problem of edge detection based segmentation techniques however is they have less performance in low intensity variation borders or edgeless images. In addition, they are poor segmentation techniques specially for noisy images.

Bottle Neck Detection and Ellipse Fitting Segmentation

Bottle neck detection and ellipse fitting segmentation techniques are also applied for segmenting overlapping cells [23]. At low magnification, cells resemble compact particles and it may be wrongly counted as one cell. These algorithms are found to have good performance in segmenting such type of cells. Bottle neck detection is used to first detect the overlapping cells and then for further splitting the cells, ellipse fitting technique is implemented. After applying these segmentation techniques on such cells, edge modification is finally applied to the broken edges during the splitting phase [23].

Segmentation Based on Clustering

Clustering techniques are also applied for cell segmentation. These algorithms start from certain group of cluster centers. And euclidean distance between the center of the cluster and the other pixels is calculated. If the distance is very near to the center, then the pixel will be grouped to the cluster and then the mean value of all pixels in the cluster will be taken as a new centroid and this algorithm continues until all pixels in the image are grouped. One major drawback of these algorithms is that, however, it is usually challenging to select the initial centroids of the image [24].

Region Based Segmentation Methods

Region growing algorithms are other type of methods that have been used for cell image segmentation. They are methods of dividing the image into different regions based on some sort of similarity criteria. This algorithms often give very good segmentation result that correspond well to the observed edges [25].

One type of region growing algorithm is watershed transform. As compared to edge detection techniques it is preferably used in noisy regions [16][26]. This segmentation technique is usually used to segment touching cells. Atta-Fosu et al. [27] applied watershed segmentation algorithm combined with the Chan-ves algorithm to segment the image of microscopically touched cells successfully.

Other type of the region growing algorithm is seeded region growing algorithm. Adams and Bischof (1994) proposed an algorithm of seeded region based segmentation technique which is controlled by set of pixels called seeds [28]. This algorithm starts from selected seed points and iteratively add connected points to form regions. In this algorithm the selection of the seed point is often difficult. Malek et al. [29] used regional and local maximum values as the first seed point in their region growing segmentation technique to segment the microcalcification in breasts. The difference of pixel intensity value and

region mean is used as a measure of similarity between the seed and its neighbors for grouping pixels to regions, i.e. the pixel with smallest intensity difference is allocated to the region. The drawback of this seed selection technique is that all local maxima pixels will be wrongly taken as seeds but there is the probability of the pixel to belong to the background region.

For the first seed selection, there are various other techniques. Some of them include competitive neural network, centroids of adjacent edges, texture features and intensity based euclidean distance. Kansal et al. [30] used histogram based techniques, i.e. the most frequently occurring pixel is taken as initial seed for region growing. The fundamental drawback of seed selection based on histogram, however, is that it does not have spatial information of the seeds, i.e. only intensity information. And this in turn may not work for some image datasets.

Even if there are varieties of cell segmentation algorithms, no single technique is sufficiently flexible and robust to accommodate some or all of the complexities that may present in cell images [22]. Major problems of most segmentation techniques especially region growing include over segmentation and under segmentations. Over segmentation occurs when more cells than expected are segmented. This is due to wrong initial seed selection or over partition of one cell into two. Over segmentation has also extra computation costs as it has additional seeds to grow. Nevertheless, if the size of the cell is known initially then over partition may be circumvented by comparing the size of a segmented cell with the standard cell size. If the size of a given segmented cell is less than the standard cell size, it may be eliminated during the post processing stage via simple thresholding. On the other hand, under segmentation occurs when some of the cells are missed by the algorithm or when two close cells wrongly considered as one cell. Under segmentation problem has no known solutions. Therefore it is usually preferable to have over segmentation rather than under segmentation [22].

A hybrid of the aforementioned cell segmentation methods usually produces a good segmentation result [9]. For example hybridizing region growing algorithm with other segmentation algorithms such as thresholding technique usually gives high accurate segmentation of medical images [31]. It is the main intent of this thesis to investigate the appication and effectiveness of a hybrid approach for use in robust analysis of OPT based cell images.

Chapter 3

Effective Analysis of Cells based on OPT Image Processing

3.1 Materials

To test the cell segmentation, human lung fibroblast cells were cultured in 3D gellan gum hydrogel scaffold for one week and prepared for imaging by Janne Koivisto (Tampere University of Technology) [32].

3.2 Image Acquisition

OPT acquires varieties of projection images at different angles depending of the desired resolution. In our case, a biological sample is placed in a sample holder and projection is taken at step angle of 0.9 degree. Full projections of an image are taken through 360 degree rotation of the sample for later 3D reconstruction. One projection of the sample is taken at step angle of 0.9 degree and that results in a total of 400 projection images captured in one full rotation [3] .

The projection images were acquired using in house built optical projection tomography setup (Computational Biophysics and Imaging group, Tampere University of Technology). A total of 2048 slices from 400 projection images were obtained using FBP algorithm. Image acquisition and reconstruction of slices were done by Birhanu A. Belay (Computational Biophysics and Imaging group, Tampere University of Technology). The OPT setup diagram is shown in Figure 3.1.

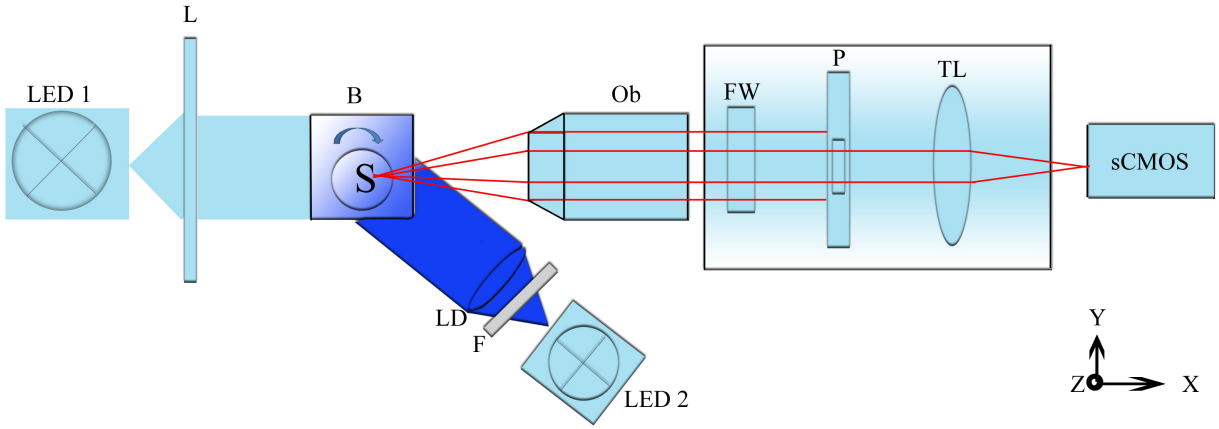

Figure 3.1: Samples inserted in FEP tubes are rotated in the rotation stage (S) inside an index matching water bath (B). A white light (LED 1) and a telecentric lens (L) are used for bright-field imaging in transmission OPT mode. Fluorescence illumination is done with 470 nm wavelength LED (LED 2), a band pass filter (F) and collimated with a lens with diffuser (LD) in emission OPT mode. The detection system consists of objective lens (Ob), a rotating filter wheel (FW) filter for a band-pass filter (used only for fluorescence imaging), a pinhole (P), a tube lens (TL), and a sCMOS camera [15].

3.3 Preprocessing

Preprocessing is used to recognize the cell regions clearly which will be convenient for segmentation. As the images are vulnerable to different artifacts and noises, preprocessing of the images is a must. First each slice of the cell images was cropped so that they will be processed fast. Simple automatic cropping was applied for this purpose. Next, the ring-like tube walls were removed simply by substituting the pixels on the ring tube walls with the median of the image. Generally the following steps were followed for removing these artifacts:

- Find center of the image.
- Calculate the radius of all pixels lying on the ring-like tube walls.
- Use equation of a cirlce to get all the pixels around the circle.
- Calculate the median of the cropped image and overwrite the value of the pixels on the ring-like tube walls with the calculated median value.

Artifacts such as spikes were common on the OPT images considered and wiener filter was used to remove these artifacts. Wiener filter was designed in such a way that the mean square error between the undegraded image (ideal image) and the restored image is minimized [17][33]. So this filter is one of the deconvolution filters that are used to restore degraded images. In the book by Gonzalez and Woods [33], the error can be mathematically stated as follows:

$$e^2 = \{x - \hat{x}\}^2 \tag{3.1}$$

where x is the undegraded image, $\hat{x}$ is the restored image and the expected value is the term inside the bracket. Minimizing this error term will give rise to the wiener filter. Accordingly, the Matlab wiener 2D adaptive noise removal filtering function was used to filter out the noises in the images. This function uses pixel wise adaptive filtering for a given window size. However, applying the same window for filtering did not work well for all image data sets considered in this thesis work. As a result, polynomial interpolation technique is used to relate the window and additive noise power on each of the images. The following steps were followed to choose optimal window to filter out the noise on each of the slice images.

- Estimate the noise power of the image.
- Find the window of the wiener filter using the polynomial interpolation formula. This polynomial relates the noise level of the image and the window of the wiener filter and it was found from the experimental data of table 4.1. Polynomial of degree seven (7) was used to relate the noise power and the optimal window. The polynomial can be described as follows:

$$W = a_0x^7 + a_1x^6 + a_2x^5 + a_3x^4 + a_4x^3 + a_5x^2 + a_6x + a_7 \tag{3.2}$$

  where W is the window of the wiener filter, x is the power of the noise and the a's with subscripts are cofficients of the polynomial which are determined from the

interpolation.

- Apply this optimal window to filter out spike noises and gaussian noises in the image using deconvolution wiener filter.

3.4 Segmentation

For the purpose of segmentation of cell slice images two algorithms were used. The first one was region growing algorithm and the second one was moving average adaptive thresholding technique. The accuracy and efficacy of the two algorithms will be compared in the result section.

3.4.1 Automatic Seeded Region Growing Algorithm

Seed based region growing algorithm performs segmentation based on the selected seed. Starting from the original seed, the region will grow based on a certain criteria of inclusion such as intensity, texture, color or frequency of occurrence of a pixel. In the region growing algorithm the first aim is to determine the initial seed point. And this step is critical for the success of the region growing algorithm.

Proposed seed selection algorithm

Seed selection method is one of the critical steps of region growing segmentation. The seed selected must be highly similar with other pixels of the region of interest (ROI) and at least there should be one seed pixel to grow to a certain region of interest. The proposed seed selection method involves spatial based intensity technique. The automatic seed selection method employed for the segmentation of the cell images can be described in the following steps:

1. Low intensity (darkest) pixels were sorted out with their coordinates from the pre-processed cell slice images. To select low intensity pixels, thresholding from the histogram image was applied [34]. This thresholding technique was related with the mean grey level of all pixels seen on the image.

2. From the sorted pixels above, iteration was done to get one representative pixel per region. This pixel was chosen based on the euclidean distance of the coordinates of the pixels. If all the pixels are within the maximum diameter of the cell, then only one representative pixel will be selected. That is, first one darkest pixel was selected. Then the euclidean distance between the pixel and all the darkest pixels was computed. If the distance is within the maximum distance of the selected pixel then only one representative pixel will be selected. So in this step only unique pixels per region were selected.

3. Group of pixels (seeds) to grow were selected. If the spatial distance (euclidean distance) between the representative pixel in step 2 and any darkest pixel in step 1 is less than the maximum diameter of the cell, the pixel will be included in the seed group or else it will be skipped. In our case, not greater than 11 pixels were used as seed group depending on the cell size, i.e. each seed will grow independently to one cell (region).

4. Grow each seed in step 3, using region growing technique which is described below.

Figure 3.2 presents the flow chart of the proposed seed selection algorithm.

Region Growing Algorithm

Region growing algorithm is described in the following steps:

1. For a given image having the seed pixel coordinates and maximum intensity difference of region pixels (in our case the difference of median of the image and intensity of seed pixel), the first step is taking the intensity of the seed pixel as the initial mean of the region to grow.

2. Check whether minimum distance between the pixel and its neighbor is less than maximum intensity distance (8 neighbor pixels are used).

3. Calculate coordinates and intensities of neighboring pixels.

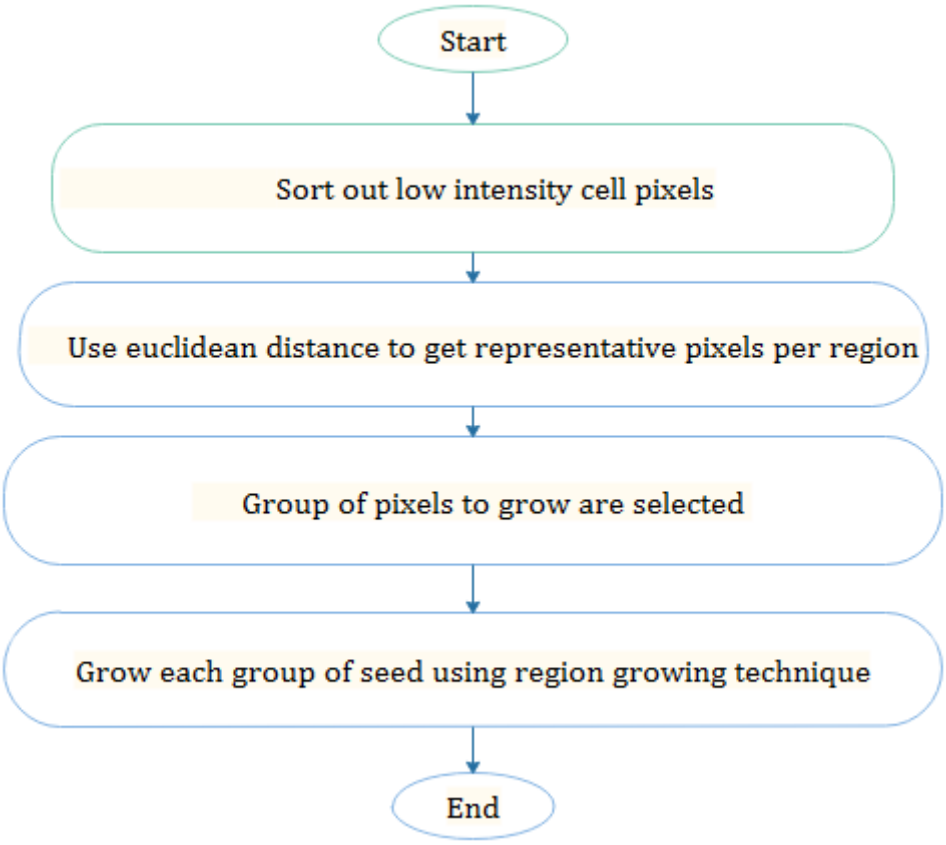

Figure 3.2: Flow chart of the proposed seed selection algorithm.

4. Check whether or not the neighbor pixels fulfill the inclusion criteria. If yes, include it in the region and go to step 5 else skip the pixel.

5. Calculate the pixel distance as the difference between the intensity of neighbour pixel and the previous mean. And the pixel with minimum pixel distance will be taken as a new seed.

6. Calculate new region mean based on the included pixels and intensity

7. Assign the new coordinates of the selected pixel (new seed) to **x** coordinate and **y** coordinate and go to step 2.

8. Repeat the process (steps 1-7) until all seed pixels in different regions grow.

Figure 3.3 presents the flow chart of the region growing algorithm.

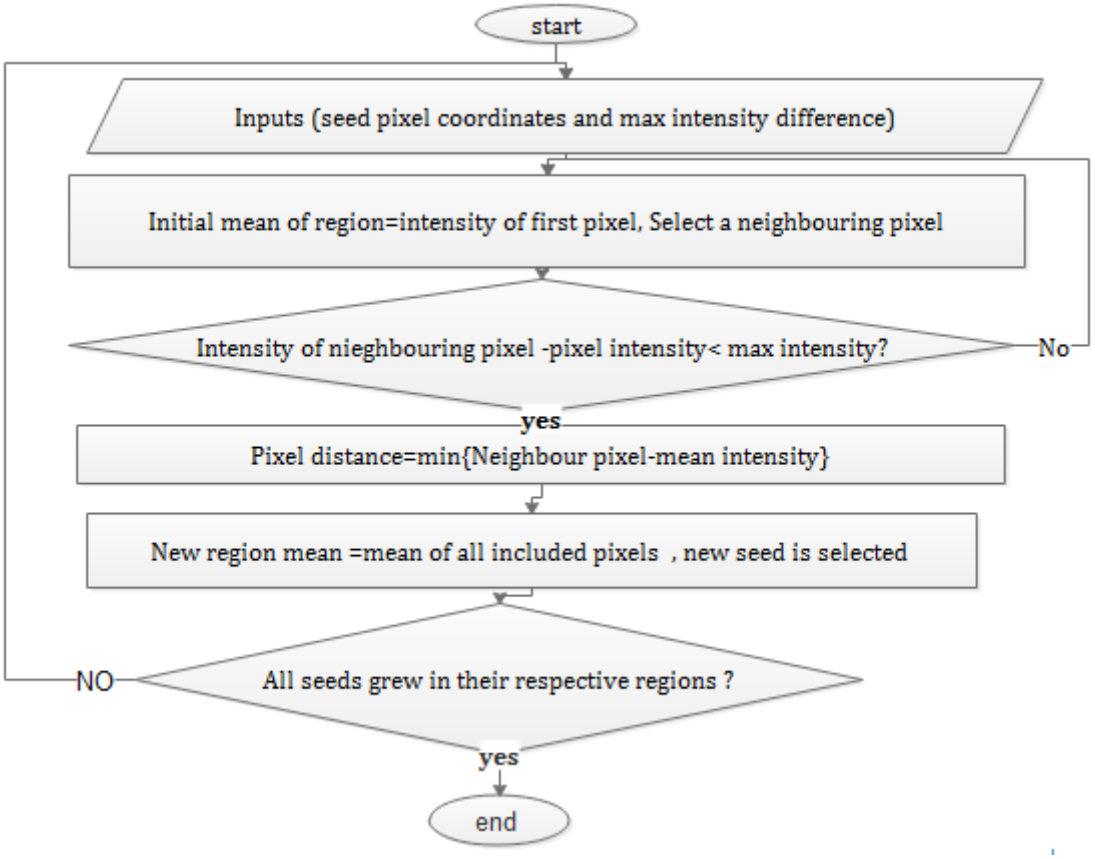

Figure 3.3: Flow chart of region growing algorithm.

3.4.2 Moving Average Adaptive Thresholding Algorithm

Moving average is the calculation of a mean of some trend from the previous mean and the current value. This means the previous mean is summed with the current value and the result is divided by two.

Researches that were done by Armstrong in 1984 and Makridakis in 1995 have shown that moving averages outperform other averaging techniques such as simple averaging , weighted averaging and exponential weighting techniques for studying market trend analysis [35]. Regarding our OPT cell images, even if the artefacts of each pixel in the cell slice images are different, they show somehow similar trends. Therefore moving average adaptive thresholding algorithm could be a preferred technique for effective segmentation of the images. As a result, the moving average of each pixel is calculated and the final moving average is taken as a threshold value for segmentation.

To determine the moving average adaptive thresholding, we assume the image as a one dimensional stream of pixels. The average intensity value of each pixel is calculated from its own intensity and the moving average of the previous pixel. After the calculation of the moving average of the first row of pixels from left to right, moving average calculation of pixels continues from right to left. This kind of scanning is called Boustrophedon scanning (scanning method of alternative lines in opposite direction similar to traditional Oxen plough). That means the pixel following the last pixel in the row i will be the last pixel in row $i+1$ and so on [34].

According to [34], The moving average of the first pixel can be calculated mathematically as follows:

$$M_i = \frac{0.5Nc}{8} \tag{3.3}$$

where: M_i is moving average intensity of first pixel, Nc is the number of columns in the image and the moving average of first pixel is taken to be approximately the half intensity value of the grey scale divided by eight [34]. Hence we are using normalized data (between 0 and 1), the half intensity was 0.5.

To determine the moving average of the rest of pixels, the moving average moves from left to right and back to left. Mathematically the moving average of the other pixels can be determined by the following formula.

$$M_{i+1} = M_i - \frac{M_i}{n} + g_{i+1} \tag{3.4}$$

where:

M_{i+1} is the moving average intensity of next pixel,

M_i is the moving average intensity of current pixel,

n is the number of previous pixel seen, and

g_{i+1} is the intensity of next pixel whose moving average is to be calculated.
Once, the moving average of all the pixels is done. The average threshold of the image is calculated as follows:

$$Threshold = \frac{M_l}{n} \times \frac{100 - pct}{100} \tag{3.5}$$

where, M_l is the moving average of the last pixel of the image and *pct* is the fixed percentage value. The value of *pct* is taken to be 23 for the specific OPT cell image threshold calculation considered in this thesis which was choosen experimentally. To determine the *pct* value, numbers from 0 to 100 were tried for the last threshold value calculation. Accordingly, a pct value of 23 works successfully to get the optimum threshold value for segmenting all the slice images. The value of *pct* was chosen experimentally also in other studies [34]. Every pixel which is less than the adaptive threshold calculated above is assumed to be the pixel of the cells. Then this optimal threshold value is applied to segment the cells. The likely pitfall is that searching and getting the fixed percentage value of the images experimentally is challenging.

3.5 Post Processing

In some of the segmented images, holes were observed and the Matlab inbuilt function $imfill$ was implemented to fill these gaps. And dilation operators such as closing were used. Also during the post processing stage, the *regionprops* inbuilt Matlab function was used to calculate area, perimeter and mean of the segmented region.

To calculate area of segmented images, the following steps were used.

- First the segmented image is converted to binary;
- The segmented binary image is labeled;
- Region boundaries of the segmented images are determined;
- Area (number of pixels) in each segmented region is finally calculated.

3.6 Stacking Segmented Images to 3D

3D Visualization, processing and measurement were done both on imageJ and Matlab. The segmented image sequence can be imported and the 3D image can be visualized using 3D Viewer or 3D volume of plugin menu in imageJ [36]. To stack segmented slices using matlab, the following general procedures were followed:

1. First 3D matrix was created using the segmented slices, i.e. empty 3D matrix was created and then segmented slices were stored in the 3D matrix.

2. Then the 3D matrix was passed to the Matlab inbuilt function $isosurface$.

3. And then the inbuilt Matlab function *patch* was applied to stack the segmented slices into 3D.

Rough schematic of the complete image processing algorithms proposed in this thesis are shown in Figure 3.4.

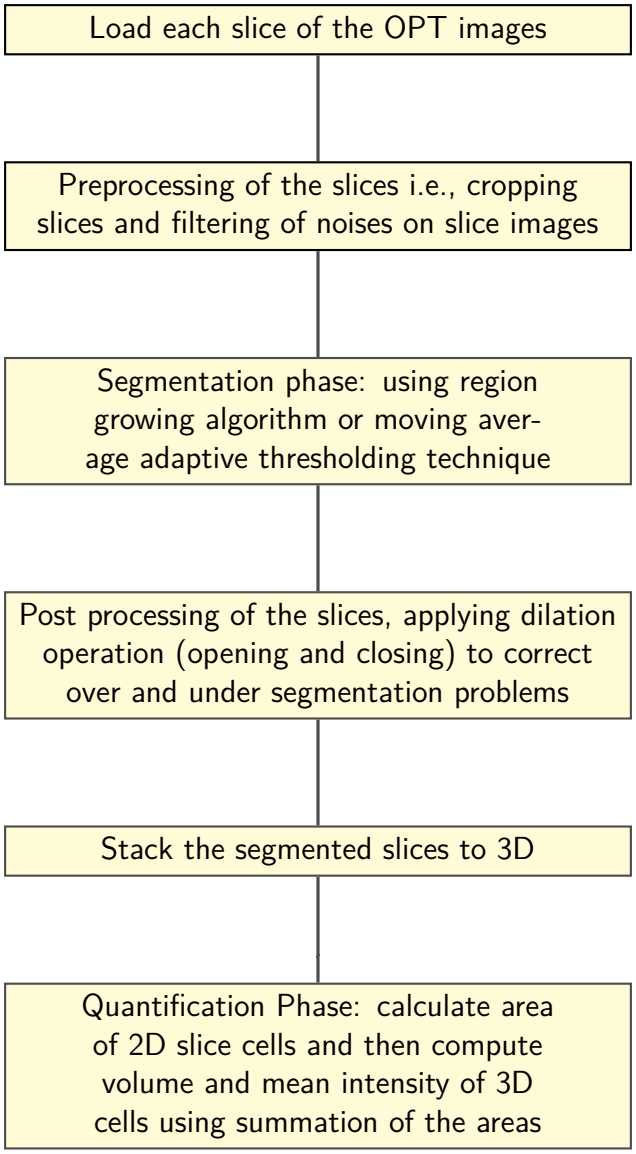

Figure 3.4: Block diagram of the proposed scheme.

3.7 Volume Quantification

For quantifying the volume of each of the 3D cells, two methods were used.

In the first method, the procedure listed below was followed.

1. Calculate the volume of part of the cell in a slice image. The volume of the cell part in one slice can be estimated by multiplication of the area of the cell part by the slice thickness.

2. Calculate volume of the cell part in all the slices where the cell part exists.

3. Sum all volumes of cell parts in step 2 to get the total approximate volume.

In the second method, the following procedure was followed.

1. Stack the slices to 3D.
2. Find the centroids of each of the 3D cells.
3. Label each of the 3D cells based on the location of their centroid.
4. Calculate the volume of each labeled cells in step 3.

3.8 Deconvolution of 2D Projection Images

Limited depth of field for high resolution OPT leads to tangential and radial blurrings in the reconstructed OPT projection images. Resolution of OPT images depends on the numerical aperture and the wavelength, i.e. it depends on the size of the airy disk according to the following formula.

$$r_{Airy} = \frac{0.61 n\lambda}{NA} \tag{3.6}$$

where: n is refractive index, λ is wavelength r_{Airy} is the radius of the airy disk and NA is numerical aperture of the lens. And the depth of field (DOF) is inversely related with the resolution according to the following formula.

$$DOF_{max} = \frac{1.305 n\lambda}{NA^2} \tag{3.7}$$

Based on the relation given in equation 3.7, for high numerical aperture lens system the depth of focus is low and this leads to blurring of reconstructed images. Other ways of reconstruction methods should be available to work around the blurring issue. Recently a way of OPT image reconstruction based on calculation of the point spread function has been suggested [4]. The method is briefly explained below.

Point Spread Function (PSF) Calculation and Deconvolution

Recently, Trull et al. [4] used the 2D gaussian PSF for use in iterative reconstruction of OPT images using the following formula.

$$h(x,z)^2 = \frac{1}{\sqrt{1+\frac{z^2}{z_R^2}}} e^{\frac{-x^2}{wo\sqrt{1+\frac{z^2}{z_R^2}}}} \tag{3.8}$$

where wo is beam waist, x is the x axis ,z is the z axis, $h(x,z)^2$ is 2D gaussian function along the y direction and z_R can be mathematically expressed as follows:

$$z_R = \pi \frac{wo^2}{\lambda} \tag{3.9}$$

where wo is beam waist (gaussian amplitude defined as $1/e$ of value of field amplitude in focus) and λ is the wavelength.

By applying the PSF function in equation 3.8 (with appropriate parameters mentioned on the result section), we could deconvolve the projection of OPT images to enhance the appearance of the cells during image reconstruction. For the deconvolution, we applied the Richardson-Lucy algorithm [33].

Chapter 4

Results and Discussion

4.1 Preprocessing

The OPT image data set consists of 400 projection images. A total of 2048 slices were reconstructed from 400 bright field projection images. Even if the cells in all slices are uniformly distributed through out the sample, there are no cells around the periphery of the cell images and hence simple automatic cropping of the images with an optimal radius should get ride of regions with few or no cells present. As a result of cropping, the size of the original image slice was reduced from 1700×1700 to 1301×1301. The effect of such cropping has been demonstrated in Figure 4.1. To know the distribution

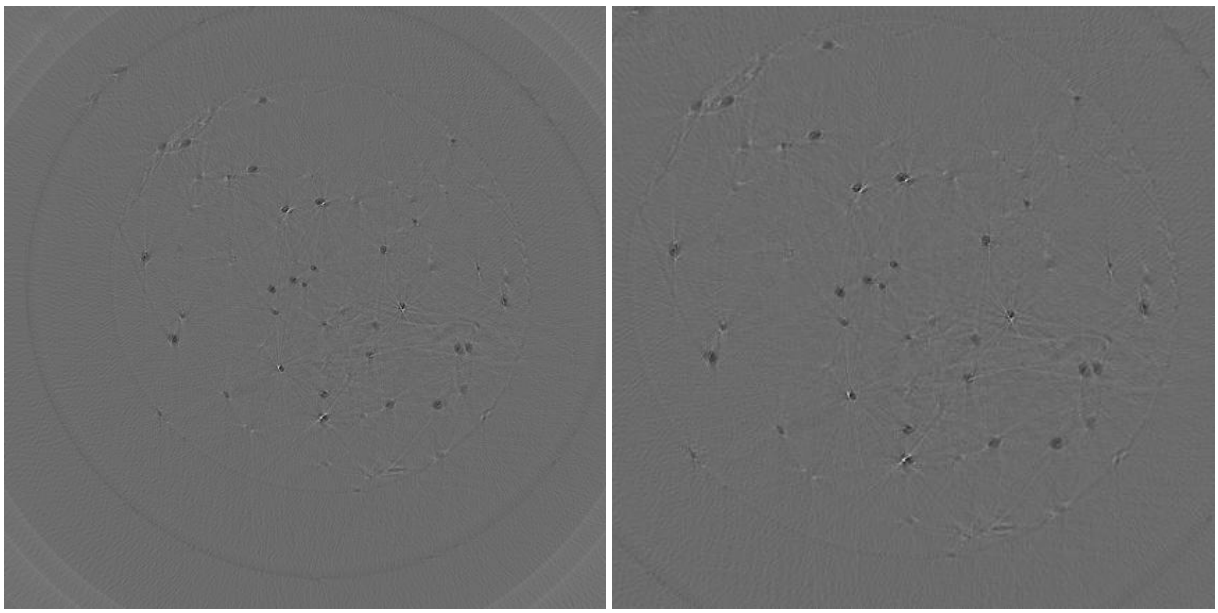

(a) (b)

Figure 4.1: (a) Original cell slice image, and (b) Automatically cropped image.

of pixel intensities, histograms of the slices were plotted. The histogram of most of the slices behaved similar to the one depicted in Figure 4.2. The pixel normalized grey level intensities are mainly concentrated between 0.37 and 0.48. On original cell slice images, there were ring shaped tube holes. For ease of latter processing stage, the pixel values

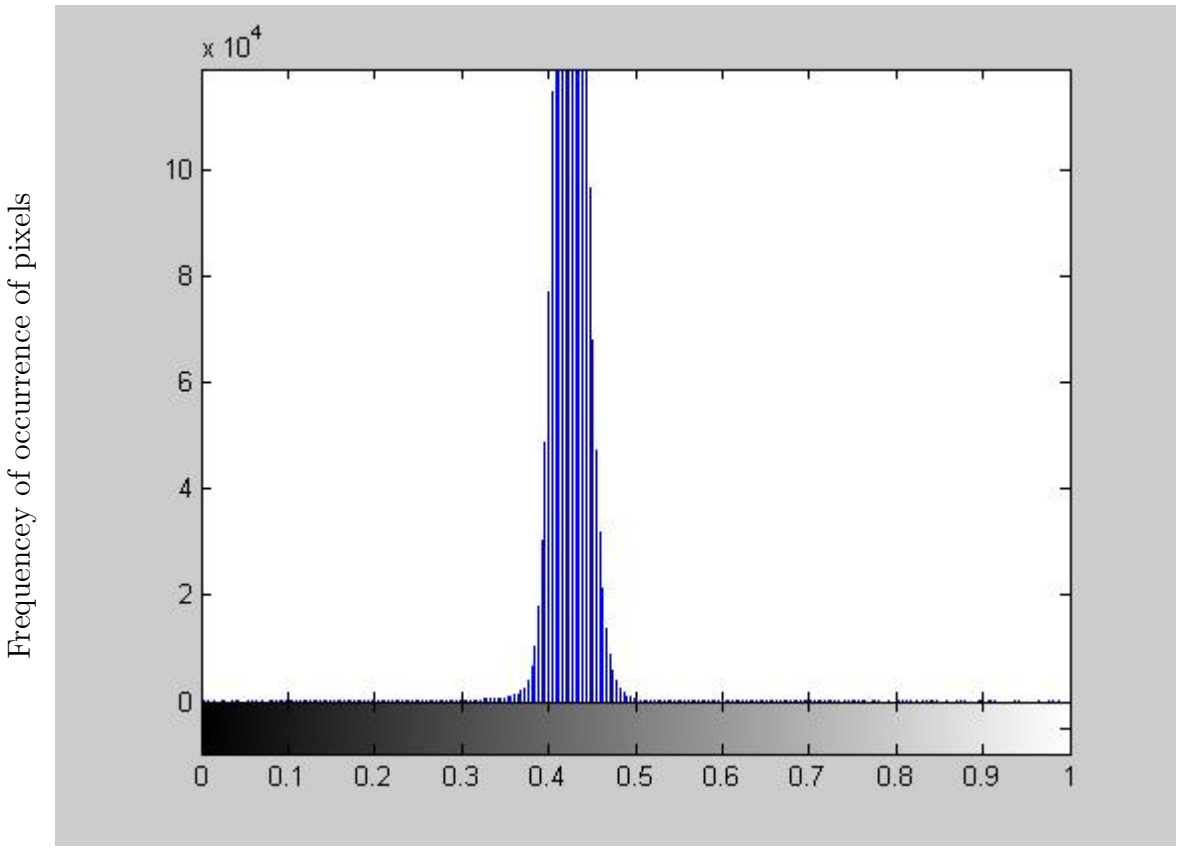

Figure 4.2: Typical histogram of cell slice images.

located on the ring-like tubes were substituted by the median value of the slice images for the first few slices.

The ring outside the cell images is removed to speed up the segmentation process. The ring tube has certain horizontal thickness and some cells were visible on the ring-like tubes, particularly for those slices located around the middle of the 3D image stacks. For that reason only pixel intensities located outside the outer ring were replaced by the median of the original image not to affect intensity values of the cells. Figure 4.3. compares two OPT image slices before and after removal of the ring-like tube walls.

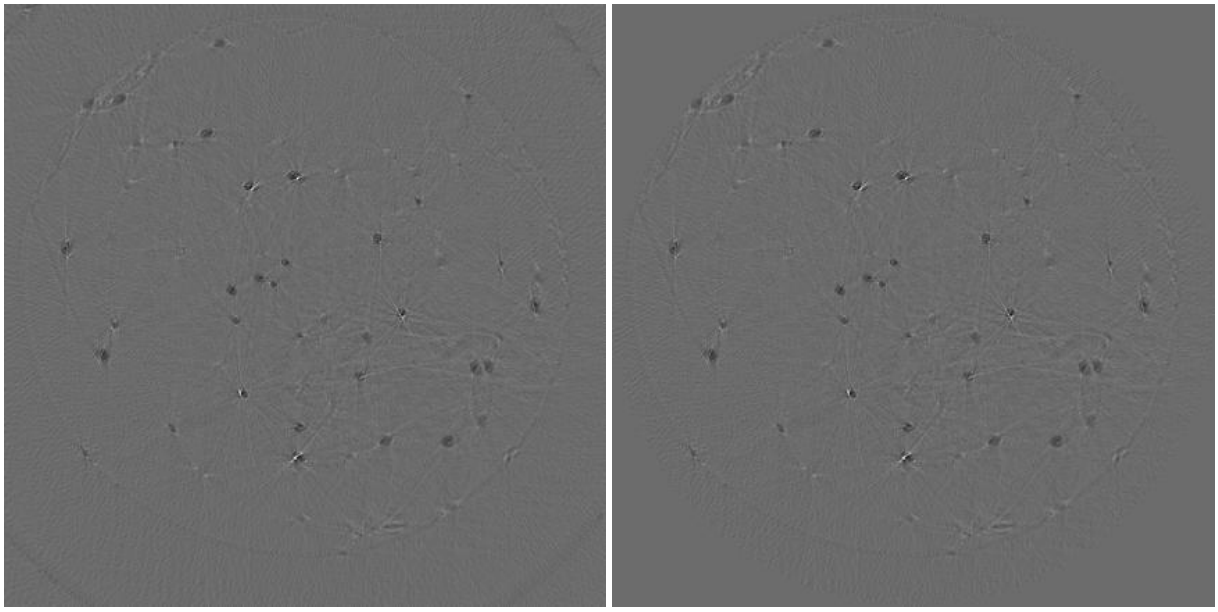

(a) (b)

Figure 4.3: (a) Original cropped image, and (b) Image after removal of ring-like tube walls.

In the original cell slice images, there were spikes specially around the cell areas. In order to remove the spikes and other additive noises, adaptive wiener filter was applied on each slice. The adaptive wiener filter also calculates the average adaptive noise of the cell slice images and the window of the filter for specific images was calculated from the average adaptive noise of each slice. Based on experiments done on the image slices to choose the best correlation function, it was found that the noise level and the adaptive local window were best related with a degree seven polynomial fitting function. For demonstration purpose, the adpative wiener filter applied on the very last OPT reconstructed slice (the 2048'th slice) is presented on figure 4.4. As shown in the figure, the additive noise and spike like structures seen on the original image are significantly removed (based on a visual assessment) on the filtered counterpart.

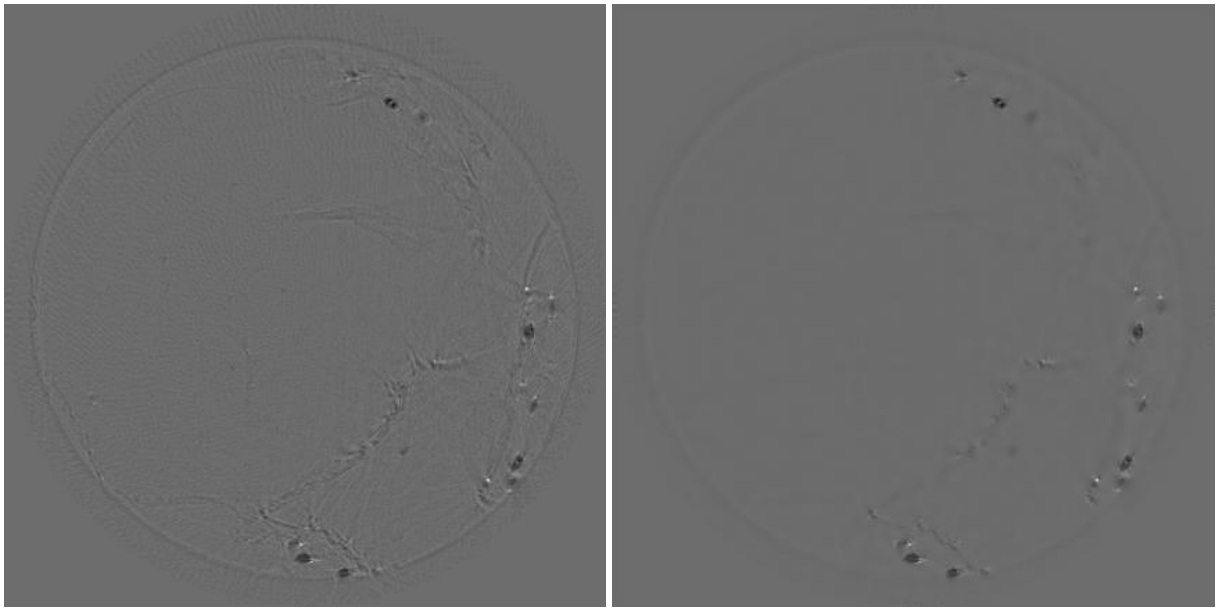

(a) (b)

Figure 4.4: (a) Original cropped image, and (b) Filtered image using adaptive wiener filter.

Table 4.1 presents the optimal window sizes used for typical cell image slices. The very last group of slices were generally degraded with high level of average noise (higher additive noise power) than the rest of the slices. For that reason the order of the adaptive wiener filter used to remove the degrading noise was typically higher for the very last cluster of slices. For instance the wiener filter applied on the bottom (first slice) was of order 7 while the top slice (last slice) used a wiener filter of order 23. The slice numbers in table 4.1 were taken randomly for demonstration purpose just to show the relationship between the average power noise and the size of the wiener window. As can be seen on the table as the average slice image noise power increases, as the order of adaptive wiener filter increases. In all cases wiener filter was effective in reducing the noise.

Slice number	1	301	650	920	1950	1970	2048
Average power of noise per cell	0.138	0.166	0.152	0.159	0.273	0.299	0.401
Wiener windows applied for filtering	7	7	7	7	17	21	23

Table 4.1: Relationship between average noise/cell and local window of adaptive wiener noise removal filter.

4.2 Segmentation

4.2.1 Simple Thresholding

Intially simple thresholding was applied for segmentation. The result of applying a simple thresholding (with a manually set threshold value which was chosen based on the histogram information given in Figure 4.2) on a cell image slice found around the bottom part of the 3D stacked image is depicted in Figure 4.5. An advantage of simple thresh-

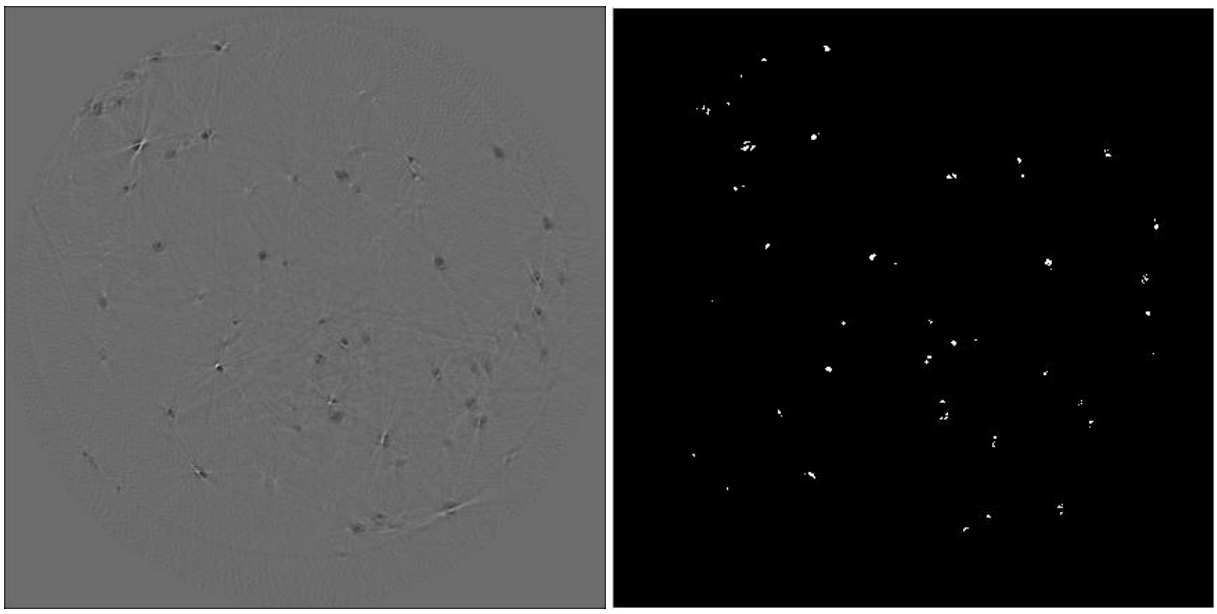

(a) (b)

Figure 4.5: (a) Preprocessed image, and (b) Segmented slice image using simple thresholding.

olding is mainly its simplicity to be applied as it only requires selection of a threshold. If the same threshold has to be applied to segment many slices, it will result in wrong segmentations. For that reason, one should manually select the right threshold value that works for a given cell image slice. The approach is truly cumbersome as well as lacking robustness. A better thresholding scheme should result in more accurate and robust outcomes.

4.2.2 Automatic Seeded Region Growing Algorithm

Figure 4.6 compares the efficacy of the automatic seeded region growing algorithm with that of simple thresholding approach presented here for demonstration. The simple thresholding approach missed to segment a number of cells that appeared on the original image while the region growing algorithm was able to detect all of them. The simple thresholding scheme very much fragmented the cells while the region growing approach offered more compact results. The performance difference gets more pronounced when dealing with cells surrounded by a high level of noise in which case the region growing approach showed a much superior performance than the simple thresholding.

Incase of simple thresholding, getting the optimum threshold value is very challenging, the automatic seeded region growing approach, however, solely depends on the seed selection step. The seed selection process is explained in the previous chapter.

Even though the region growing approach offered commendable results than simple thresholding, it also comes with its own pitfalls, the major one being over segmentation issue. The method sometimes considers some non cell artifacts surroundig the cells as part of the cells which results in exaggerated cell sizes.

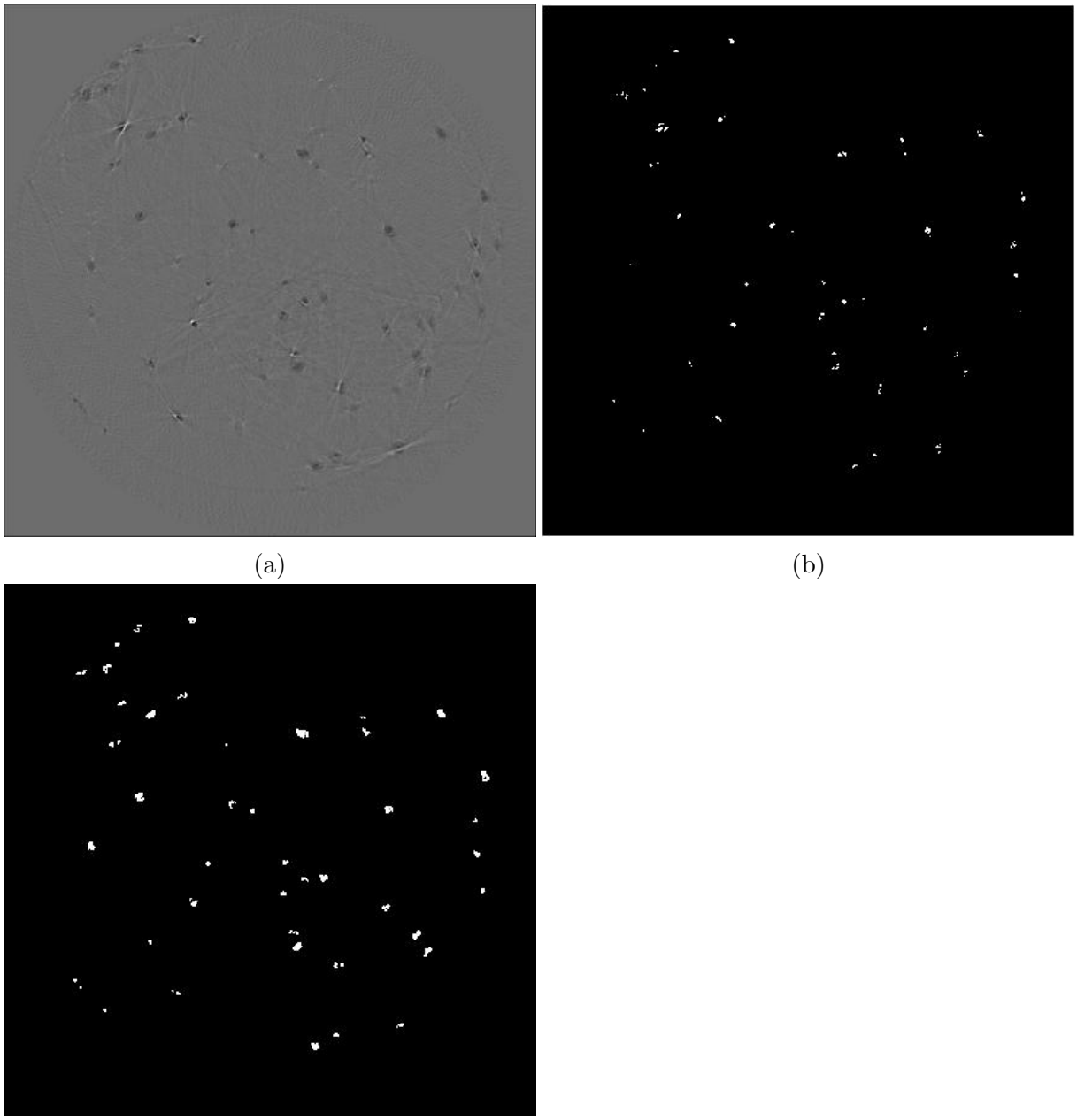

(a) (b)

(c)

Figure 4.6: (a) Preprocessed image, (b) Segmented slice image using simple thresholding algorithm, and (c) Segmented slice image using ASRG.

4.2.3 Moving Average Adaptive Thresholding Technique

Moving average adaptive thresholding technique has better robustness compared to simple thresholding technique and automatic seeded region growing technique. As demonstrated with examples, the approach offered better results when dealing with cell images with a great deal of noise content in them.

Figure 4.7 compares the performance of the automatic seeded region growing algorithm with that of the moving average adaptive thresholding scheme on two selected cell image slices. The segmentation results clearly shows that there is a considerable difference between the two approaches. Based on a qualitative (visual) assessment of the two results, it was found out that the region growing approach over segment cells particularly in cases where the cells are surrounded by pronounced noise artifacts and spikes. Note that two consecutive slices taken from the 3D volume were considered in figure 4.7 to compare the two algorithms.

Moreover, the size of segmented cells in automatic seeded region growing algorithm are greater than that of the moving average thresholding. And this in turn will have an effect in the 3D visualization later.

The image subtraction result of the two algorithms is depicted in figure 4.8 below.

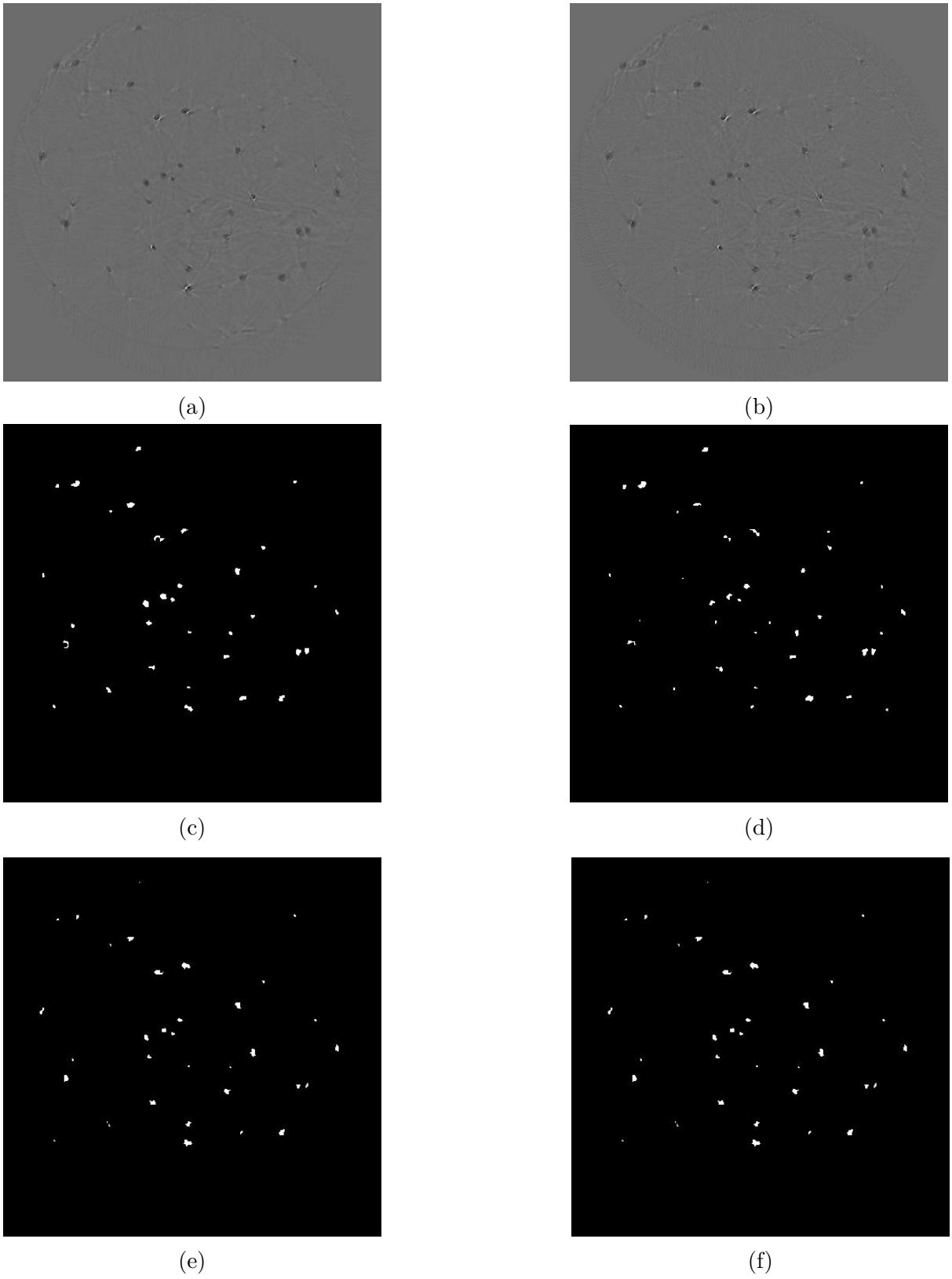

(a) (b) (c) (d) (e) (f)

Figure 4.7: (a) Preprocessed image of slice 1, (b) Preprocessed image of slice 2, (c) Segmented image of slice 1 using ASRG, (d) Segmented image of slice 2 using ASRG , (e) Segmented image of slice 1 using MAAT, and (f) Segmented image of slice 2 using MAAT.

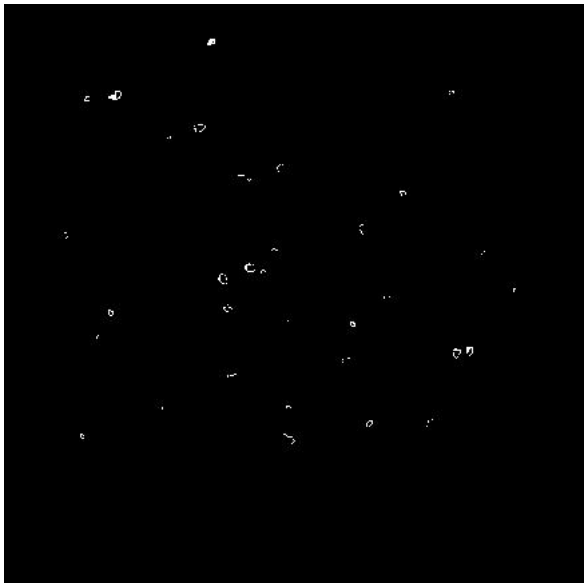

Figure 4.8: Image subtraction result of moving average adaptive thresholding and automatic seeded region growing algorithm (region growing-moving average).

4.3 Post Processing of Cell Slice Images

Even if a segmentation technique with better accuracy was applied on each slice images, it was common to see few discontinuities around some of the segmented cells. This discontinuity may appear on the image either due to unresolved spike noise during the preprocessing stage or due to the very low intensity and resolution of cell part during image acquisition. As shown on the original image in Figure 4.1, for example, cells with spikes have very bright pixel intensities (spike noises). Unless these spikes are removed, these regions will most likely create gaps during the segmentation phase. Adaptive wiener filter minimizes these noises significantly, however, it is challenging to remove these noise completely as it will affect the whole cell region. Moreover, in some cells it was common to see very low intensities either around the border of the cells or around the central region of the cells. This might happen due to the resolution of the OPT or due to the scientific Complimentary Metal Oxide Semiconductor (sCMOS) camera detectors.

Therefore it was essential to apply post processing techniques to circumvent the above mentioned challenges. The following steps were followed accordingly. First an average

distance between discontinuity pixels was calculated. Next simple dilation operators such as closing was applied on the image to close the gaps between the splitted cell parts. And then the inbuilt matlab function imfill was employed to significantly minimize the discontinuity (gaps).

Moreover, during the segmentation of slices, there are particles which have highly similar intensities with the cells in the slice. The particles typically are smaller in size than cells. Hence based on size features, Matlab *ismember* built in function was used to eliminate the particles. Figure 4.9 presents the segmentation performance of the moving average scheme after the application of the imfill (post processed image). Broken cell segments appeared to be joined after the $imfill$ function was applied.

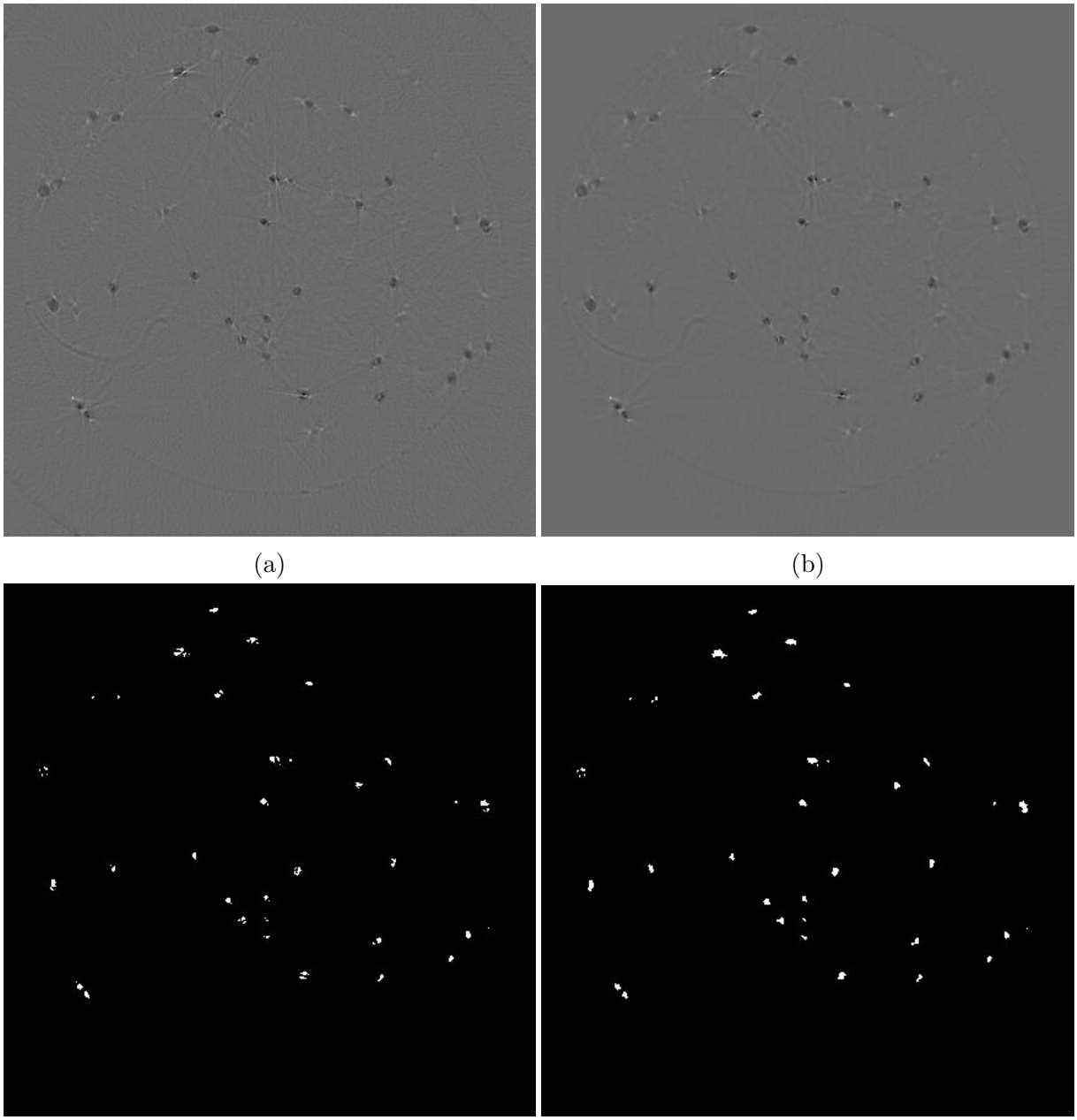

(a) (b)

(c) (d)

Figure 4.9: Post processing result: (a) Original cropped image, (b) Preprocessed image, (c) Segmented image using moving average, and (d) Postprocessed image.

4.4 Slice Based Cell Counting and Cell Area Calculation

In 3D cell culture, quantification of number of cells is required to analyze how many cells are grown and how many new cells are emerging out. To count existing cells, first all cells need to be labeled . The labeling is done from right column to left. This was done using the Matlab built in *bwlabel* function. The number of cells in a given slice is then

simply the maximum number of labeled cells in that slice.

The area of each cell was also computed using Matlab following the steps previously explained in chapter 3. Figure 4.10 presents the labeled cells of first slice for calculating the area of each cell.

(a) (b)

Figure 4.10: Matlab based area calculation: (a) Segmented slice of automatic seeded region growing for area calculation, and (b) Segmented slice of moving average adaptive thresholding for area calculation.

Table 4.2 compares cell areas computed using the Matlab based scheme explained in this thesis applied on segmented images using MAAT and ASRG method. In most cases the region growing method tends to over estimate the cell areas. This is consistent with the segmentation result obtained from the two results in which case the ASRG scheme tends to over estimate the cell regions than the MAAT scheme.

Cells	1st cell	2nd cell	3rd cell	4th cell	5th cell	6th cell	7th cell	8th cell
Cell area (MAAT method)	166	27	42	266	57	4	98	12
Cell area (ASRG method)	83	93	137	36	132	391	34	79

Table 4.2: Cell numbers and their corresponding area in pixels matlab result for moving average adaptive thresholding and automatic seeded region growing algorithm.

4.5 3D Stacking and Analysis Using MATLAB

3D volumetric Visualization of cells is one interesting aspect in 3D cell culture studies. The segmented 2D slices need to be stacked along the z direction for a complete 3D visualization. In this thesis 3D volume stacking was done using the following quick procedures. First all slice images were copied to a 3D matrix, next the Matlab built in *patch* function was used to stack the 2D slices along the z direction. One thing to note here was that the stacking was generally a computationally intensive procedure to be implemented on ordinary computing device with small number of cores. This limits the number of segmented OPT reconstructed images that need to be visualized in 3D. Figure 4.11 presents both the top as well as the side views of a 3D stacked group of segmented OPT slices.

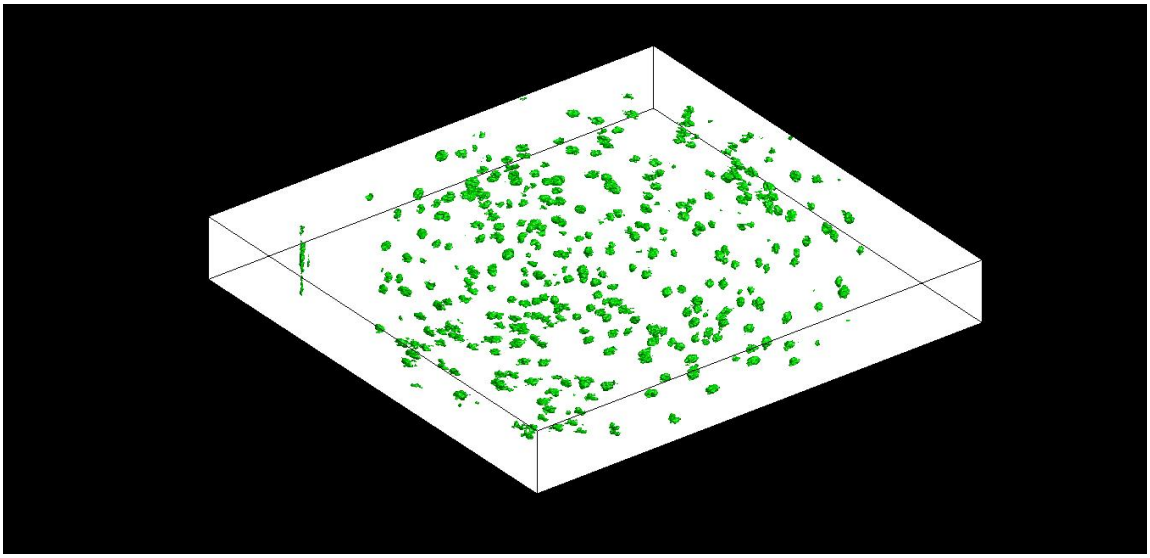

(a)

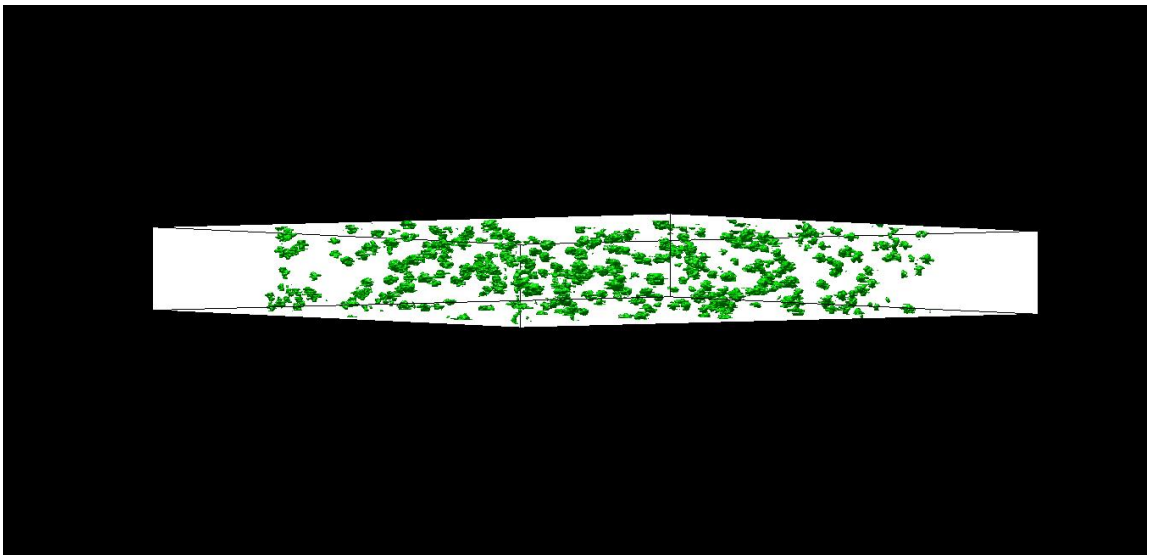

(b)

Figure 4.11: Matlab 3D stacking results: 3D stacking of 150 segmented cell image slices top view (a) and side view (b).

4.5.1 Volume Quantification in Matlab

To quantify the volume of each cell in 3D, each of the 3D cells are labeled with numbers and then the volume of the labeled cell images is calculated. The labeled 3D cells of the first 20 stacked slice images is shown in Figure 4.12 below.

The volumes of the first 7 labeled cells are shown in Table 4.3 below.

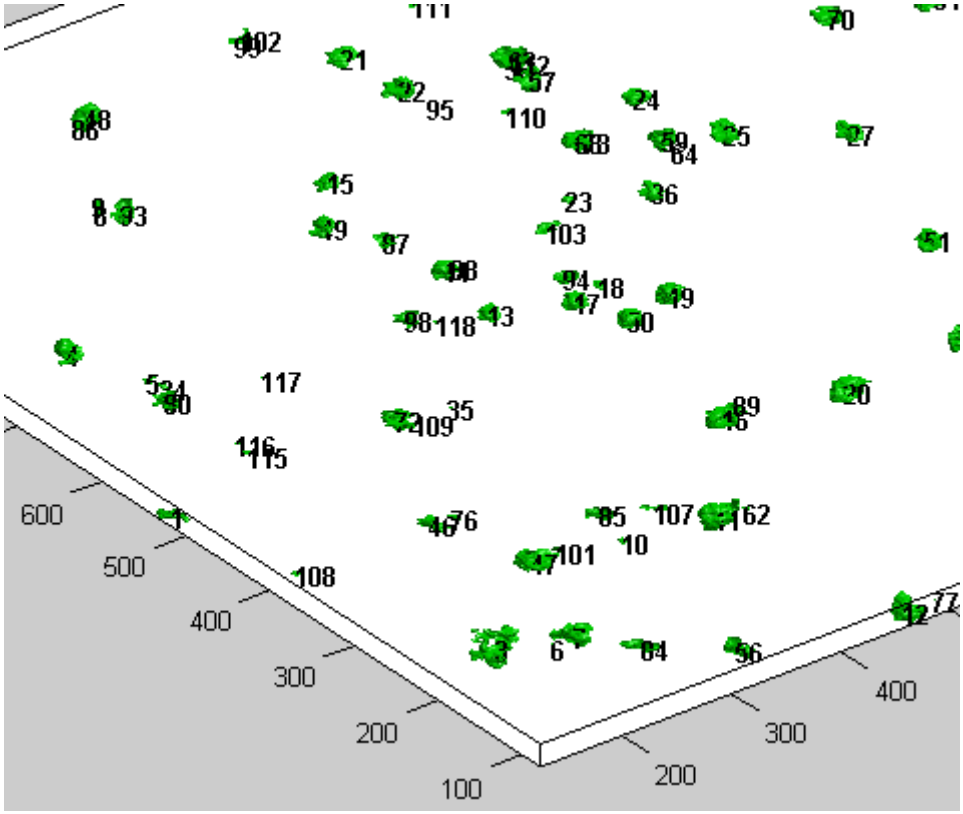

Figure 4.12: 3D labeled cells for volume quantification

3D Cells	1st cell	2nd cell	3rd cell	4th cell	5th cell	6th cell	7th cell
Volume (μm^3)	1201.8	1414.9	8394.7	5143.2	125.2	19.77	5228.8

Table 4.3: 3D Cell numbers and their corresponding volume Matlab result (2D segmentation algorithm: MAAT).

4.6 3D Stacking and Analysis using ImageJ

Other than Matlab, ImageJ also provides very good 3D visualization capabilities. In ImageJ, there are plugins which allow to visualize 3D data. Among all plugins, the volume viewer and ImageJ 3D viewer plugins are used to visualize the 3D stacked data from given 2D segmented slice images. The 2D segmented images are first imported to ImageJ as image sequences and stacked using ImageJ3D viewer.

Figure 4.13 presents both the top as well as the side views of a 3D stacked group of segmented OPT slices using the ImageJ plugins. Compared to Matlab, ImageJ allows stacking of more number of slices into 3D being more efficient than Matlab.

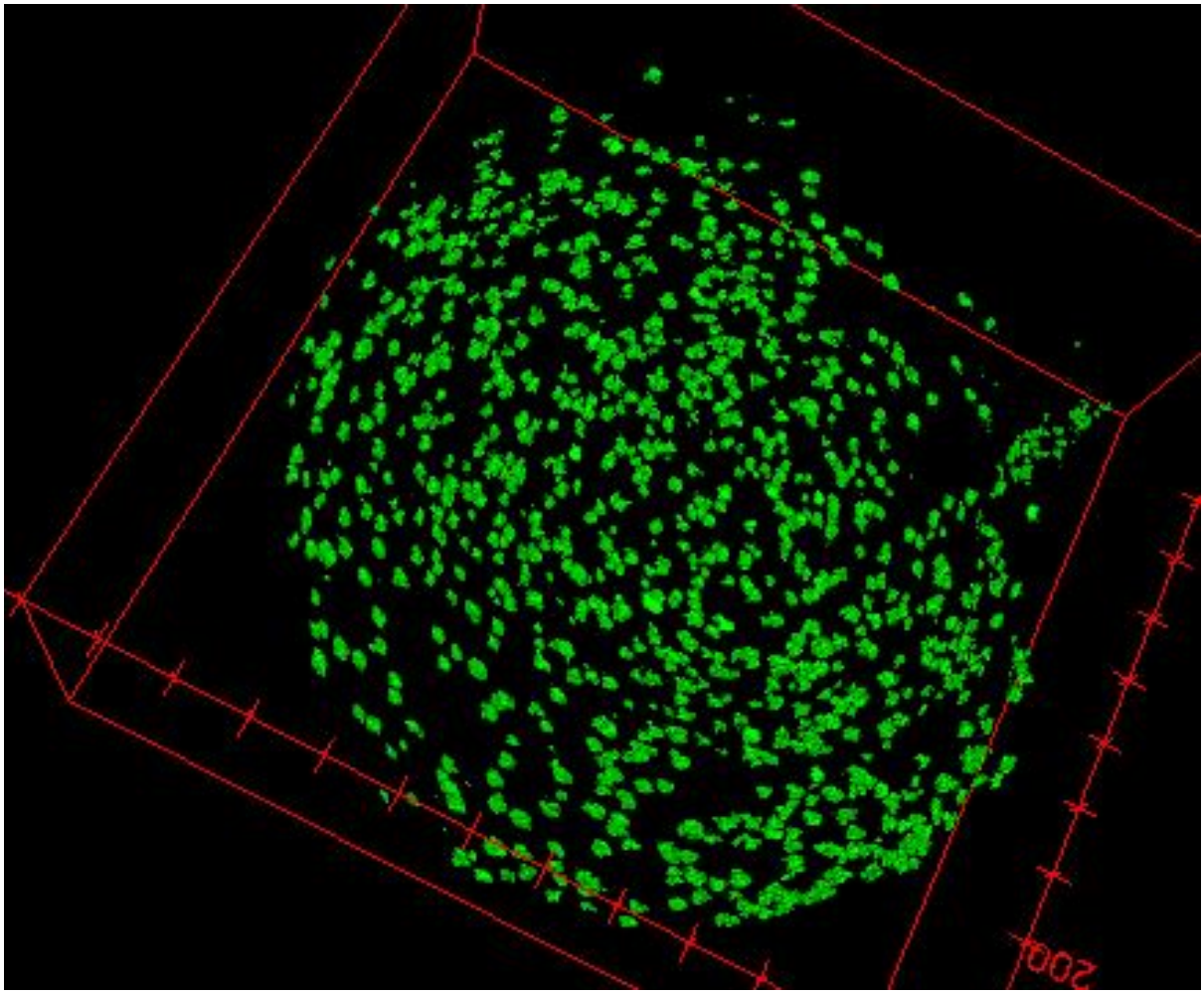

(a)

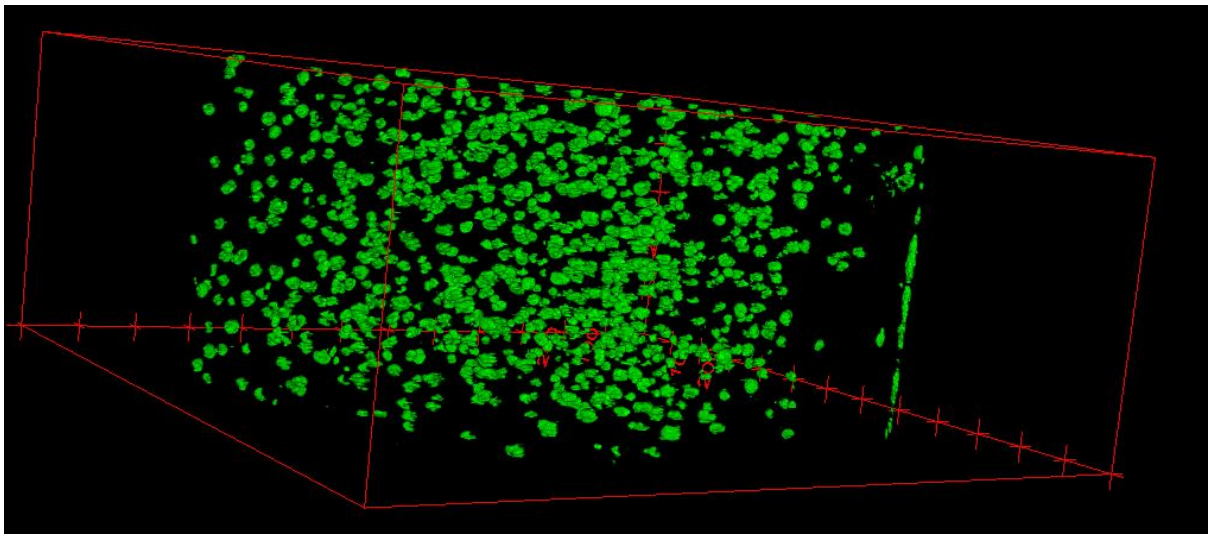

(b)

Figure 4.13: ImageJ 3D stacking results: (a) 3D stacking of 500 segmented cell image slices top view (a) and side view (b).

Figures 4.14 and 4.15 compare the 3D stacking results using ImageJ plugins for the two methods namely the region growing and moving average methods. The top view appearance using both methods might look similar. However, the side views are very different. Ideal cell shapes are close to spherical. The side view appearance on the moving average segmented images are much more spherical than that of the region growing based segmented cells. This is what was expected indeed; the 3D stacking performance mostly depends on accurate and robust segmentation of the cells in each of the cell image slices. As demonstrated earlier, the slice based segmentation outcomes of the moving average adaptive thresholding method is superior to that of the region growing scheme, the simple thresholding method being the worst performer. As a result the 3D stacking results using the moving average scheme out performed the region growing scheme. This will in effect define the overall accuracy of further 3D cell quantifications.

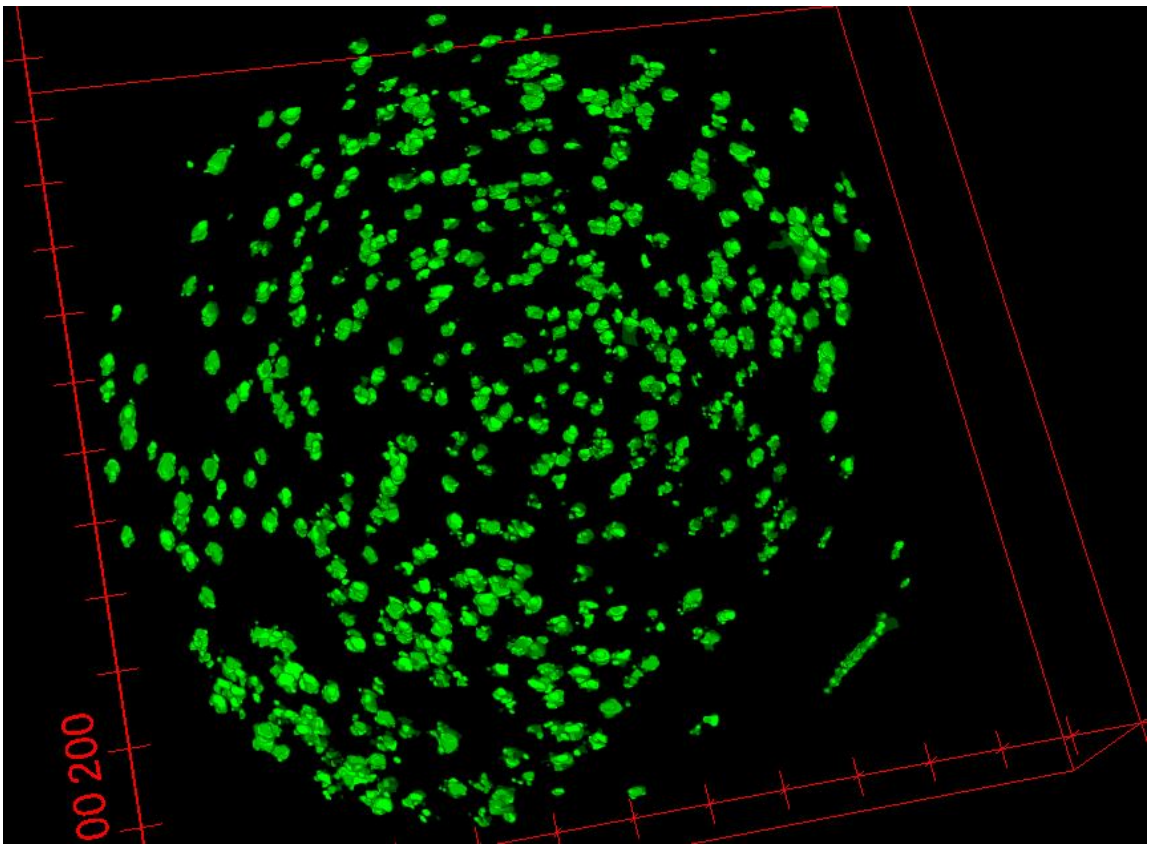

(a)

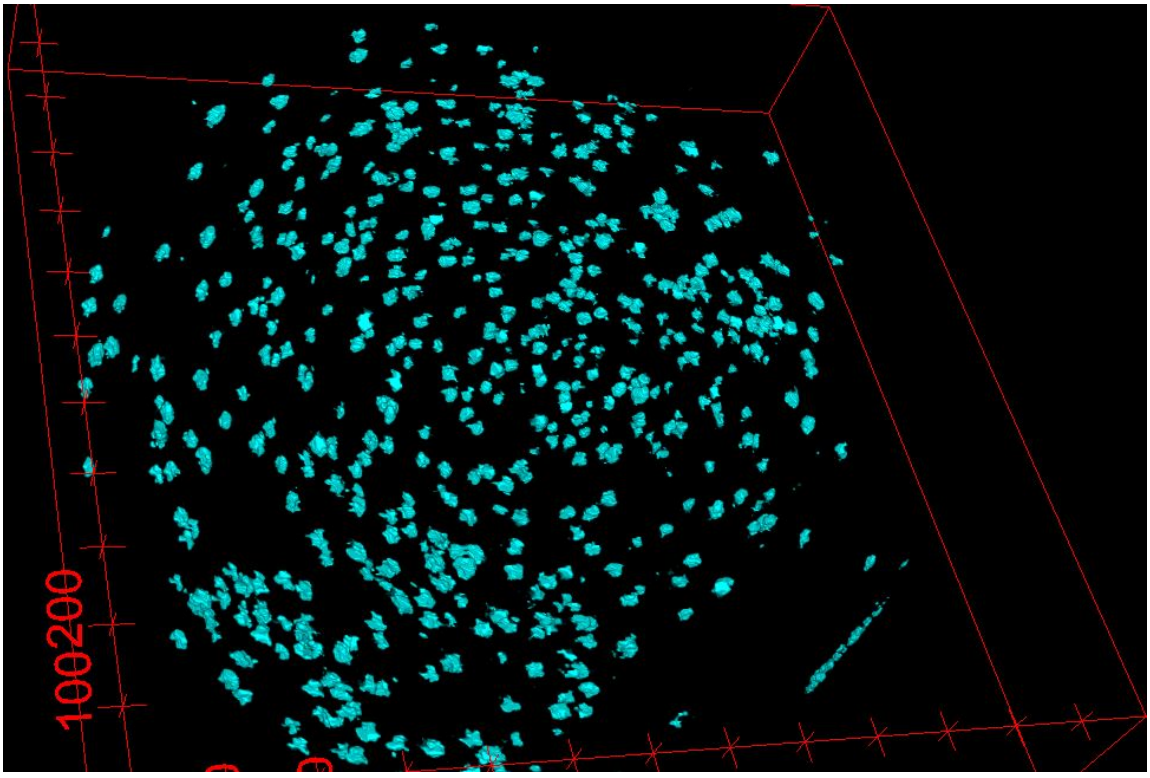

(b)

Figure 4.14: ImageJ based 3D top view visualization of OPT segmented cell image volume using automatic seeded region growing algorithm (a) and moving average adaptive thresholding method (b).

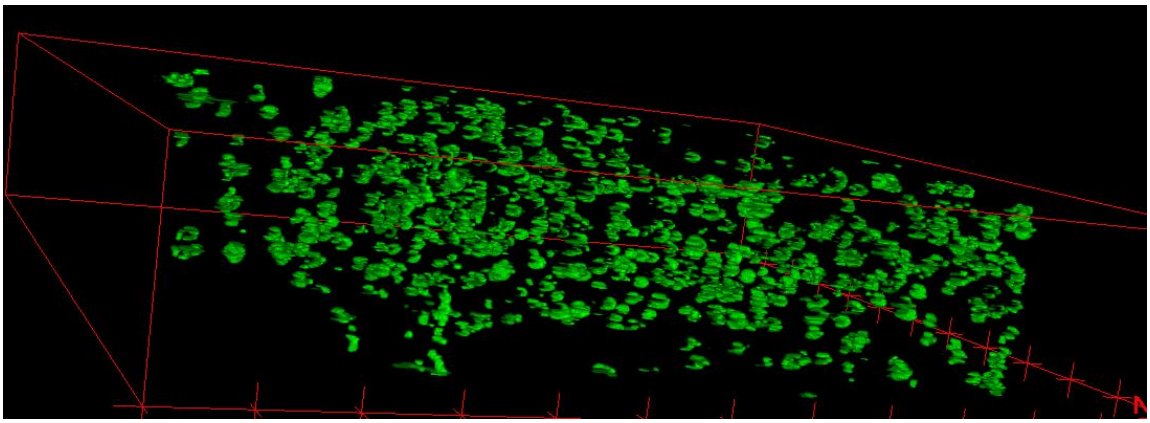

(a)

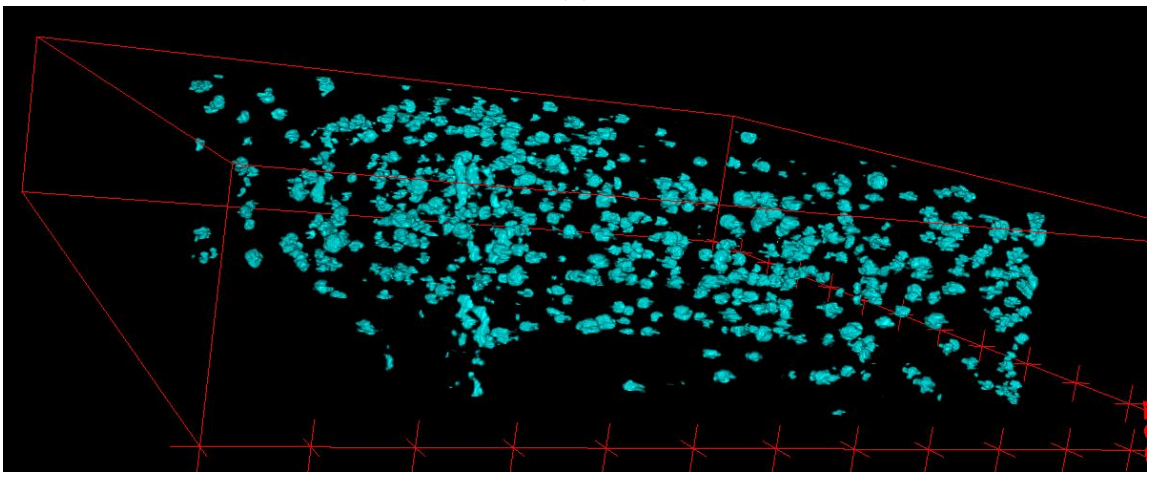

(b)

Figure 4.15: ImageJ based 3D side view visualization of OPT segmented cell image volume using automatic seeded region growing algorithm (a) and moving average adaptive thresholding method (b).

4.7 3D Volume Qauntification using ImageJ

To calculate the actual volume of each cell in ImageJ, slice based (2D based) volume calculation is followed. First, the cells on the first slice are all labeled. Note that the actual pixel dimension of all OPT images considered in this thesis was 1.3μm $\times$ 1.3μm. That means every pixel has a length of 1.3μm. This length was used as a scaling parameter for ImageJ implementation. To calculate the volume of a single 3D cell, first the area of the cell part in each of the slices wherever the cell part exists is calculated using measure stack ImageJ plugin and multipled by the slice tickness (1.3μm) to compute the volume on that slice. The sum of all volumes on each slice will approximate the total volume of the cell in μm^3. ImageJ outputs the actual volume of the cell for a specified scaling parameter.

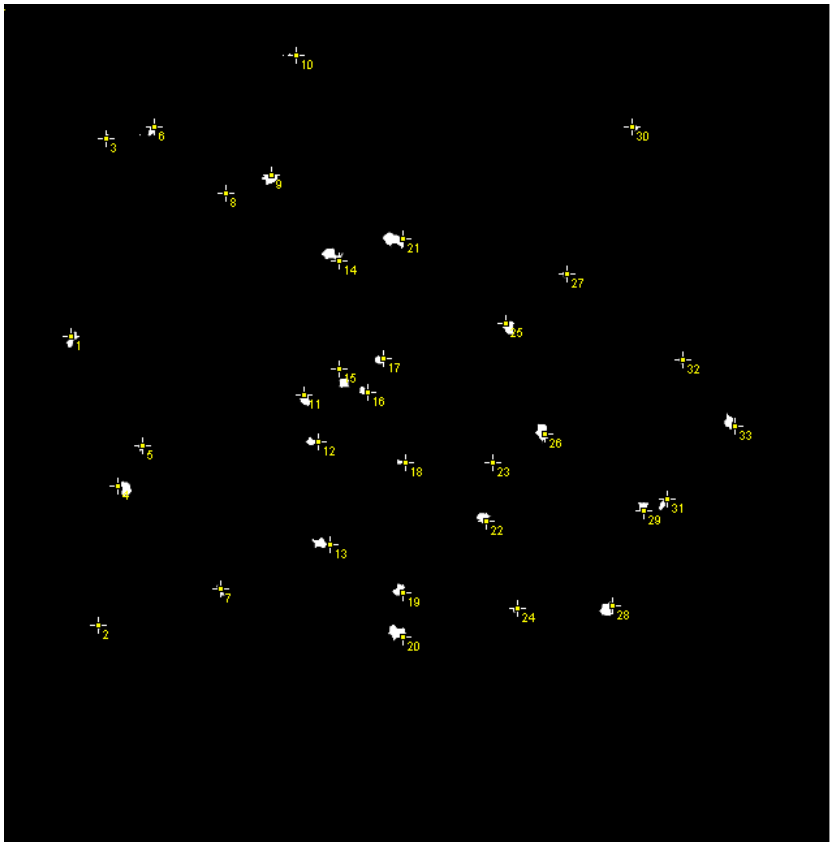

Figure 4.16: Cell Labeling applied on the first OPT cell image slice.

Figure 4.16 shows labeling of cells applied on the first OPT slice. A total of 33 cells were labeled. For example the cell labeled number 1 spans a total of 5 consecutive slices

starting from the very first OPT slice. Some statistics including volume of cell on a single slice(area× slice thickness), minimum as well as maximum intensity values for this cell on each of the 5 consecutive slices where it spans are presented in Table 4.4. The volume

Number	Volume of cell part in a single slice(μm^3)	Min intensity	Max intensity	Slice no
1	364.7	0	255	1
2	371.29	0	255	2
3	307.58	0	255	3
4	92.27	0	255	4
5	65.91	0	255	5

Table 4.4: Statistics of first cell.

of the first cell is then approximately the sum of volumes of cell part in each slice in the 5 consecutive slices as shown in table 4.4.

The actual volumes of the remaining labelled cells could be computed in a similar way. Table 4.5 presents the volumes of five selected cells computed from cell images segmented using the moving average adaptive thersholding technique as well as the region growing algorithm. Again, the region growing algorithm mostly tends to over estimate the total volume of cells. As it is shown in table 4.5, there is a considerably high discrepancy between the two methods.

Cell No	One	Three	Six	Eight	Ten
Volume (μm^3) using MAAT	1201.8	11489.0	5184.9	118.6	5523.3
Volume (μm^3) using ASRG	1507.1	16537.0	6197.0	331.7	8526.0

Table 4.5: Volume of the first 5 labeled cells in Figure 4.16 in cubic micrometer using ASRG and MAAT algorithms.

4.8 Comparison of MAAT and ASRG Algorithms

Generally the adaptive thresholding and the region growing algorithms are compared in terms of their efficiency, accuracy, size of volume of cells, area of 2D slices of cells and consistencey of segmentation as shown in Table 4.6 below.

Criteria of comparison	Region Growing (ASRG)	Moving Average (MAAT)
Accuracy	Medium	Good
Efficiency	Slow	Very fast (30x faster than ASRG)
Volume of 3D cells	Over estimated	Visually close to the actual cell volume
Area of cells on 2D slices	Over estimated	Visually close to the actual cell volume
Consistencey of segmentation	Consistent but the shape differs	Consistent
3D visualization of cells	Many cells appear irregular in shape	Less irregular in shape

Table 4.6: Comparison of the performance of the two algorithms namely automatic seeded region growing and moving average adaptive thresholding.

4.9 Result of Deconvolution of Projection Images Using PSF

Following the discussion in Chapter 3, the PSF was computed using the following OPT parameters: as OPT uses green light spectrum, the wavelength (λ) was taken to be 500nm. The calculated beam waist (wo) was $1.1368\mu m$. The full width at half maximum (FWHM) can be calculated using the wavelength and the beam waist using the formula in Equation 4.1.

$$FWHM = 1.028\frac{\lambda}{wo} \tag{4.1}$$

The sigma (standard deviation of the PSF gaussian) can be calculated from the FWHM as follows:

$$\sigma = \frac{FWHM}{2\sqrt{2\ln 2}} \tag{4.2}$$

where σ is the standard deviation.

The resulting PSF will have the shape shown in Figure 4.17 where around 99.97% of the gaussian data is located within $3 \times \sigma$ (standard deviation). As said in Chapter 3, in order to enhance the projection images using the calculated PSF, the Richardson Lucy algorithm was utilized [33]. The Matlab in built function *deconvlucy* with 10 and 400 iterations resulted in a deconvolved image that is presented in Figure 4.18. Typical differences are observed on the projection images before and after the application of the

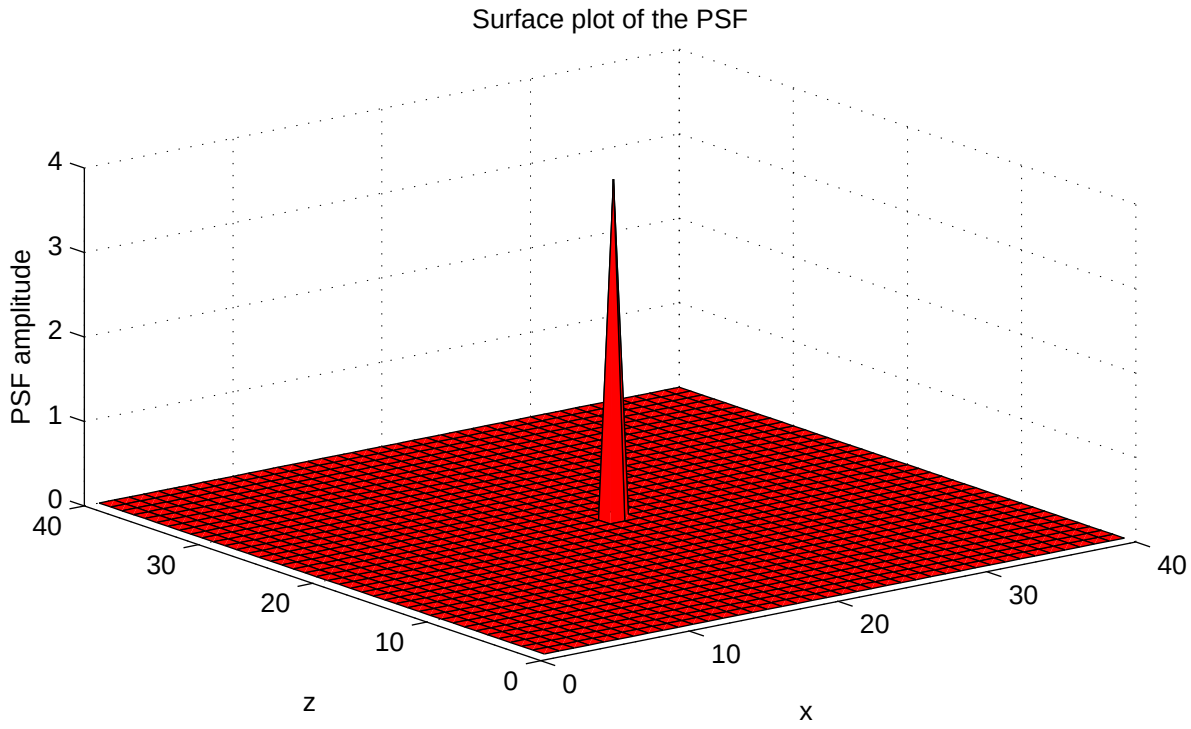

Figure 4.17: The shape of the calculated PSF.

PSF. This is so particularly in areas where spikes are visible. There is a great deal of enhancement obtained by the application of the PSF. As the number of iteration increases, the image gets more enhanced. Regions around the image boarders are corrupted due to edge effects. No effort was exerted to correct the edge effects even though there are methods already discussed in the literature on how to deal with edge artifacts and that step is beyond the scope of this thesis study.

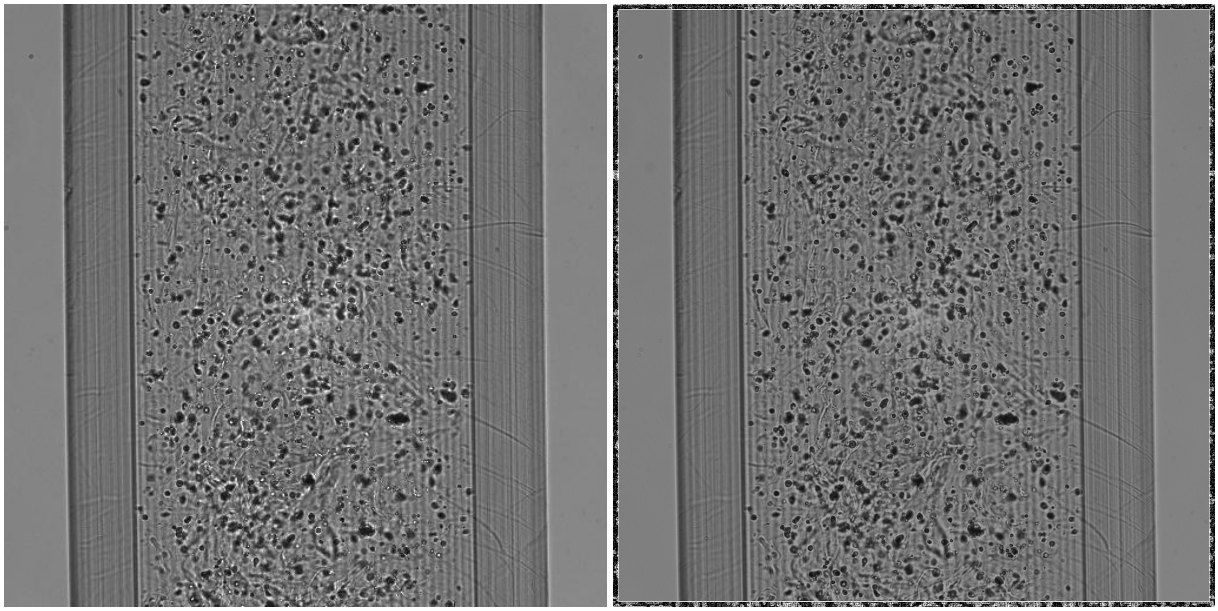

(a) (b)

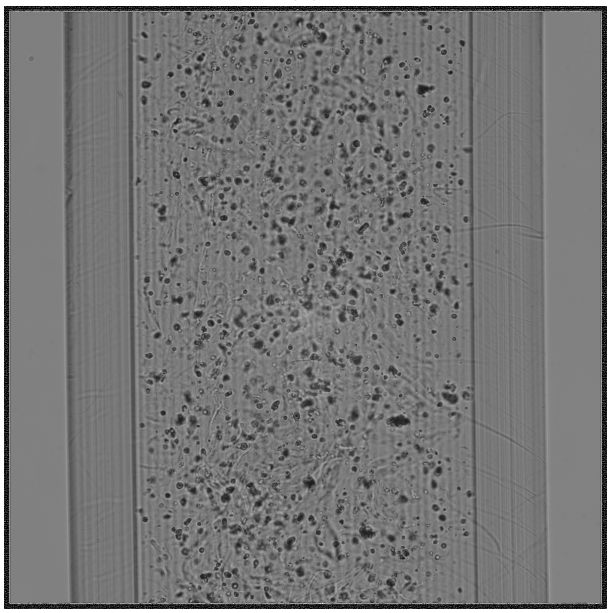

(c)

Figure 4.18: Deconvolution result: (a) Original projection image, (b) Deconvolved projection image using the calculated PSF after 10 iterations, and (c) Deconvolved projection image using the calculated PSF after 400 iterations.

Chapter 5

Conclusion and Recommendation

5.1 Conclusion

OPT is a new technique used to image cells in 3D cultured in a hydrogel. It uses standard FBP algorithm to reconstruct the images, however its use of photons in the visible spectrum urges it to have limited depth of field for high numerical aperture lens system. As a result, there are tangential and radial blurrings in the reconstructed images of OPT. In addition there are several artefacts in the reconstructed slice images of OPT. Several researchers came up with different techniques to alleviate these problems.

In this thesis work, varities of image processing approaches were applied to ameliorate the 2D slice images of OPT. For instance in the preprocessing stage wiener filter with automatic window selection technique was applied. And this significantly minimized the artefacts of 2D slice OPT images. And for better 3D visualization of cells, two segmentation algorithms namely automatic seeded region growing algorithm and moving average adaptive thresholding techniques were tested. And then segmented slices of both alogrithms were independently stacked to 3D to observe cell interactions in 3D. The 3D stacks from segmented images of the two algorithms mentioned above were carefully analyzed. Based on visual assessment of the final 3D stacked slices, it was found that the moving average adaptive thresholding scheme out performed that of the region growing approach. Generally, the region growing approach was found to over estimate cell dimensions. The complete 3D characterization and quantification of the cells was found to be highly dependent of the performance of the 2D slice based segmentation scheme.

5.2 Recommendation

Even though the segmentation technique used in this thesis work offered commendable results, there are still rooms to improve its performance particularly when it is applied to OPT slices with high degree of difficulties (pronounced level of noise and spikes). A complete 3D segmentation of the cells also could be tried instead of the slice based segmentation scheme discussed in this thesis. It is believed such a complete 3D segmentation scheme could improve not only the accuracy but also the computational efficiency as well.

The idea of enhancing OPT projections using the point spread functions discussed in this thesis is at its preliminary stage. The final reconstruction of a new set of OPT images that could be compared against the OPT data that used the natural filtered back projection scheme could be interesting to look at. Furthermore, the potential clinical implications of the results found in the thesis await further investigations.

Bibliography

[1] E. Figueiras, A.M. Soto, D.Jesus, M. Lehti, J. Koivisto, J.E. Parraga, J. Silva- Correia, J. M. Oliveira, R.L. Reis, M. Kellomäki, and J. Hyttinen, "Optical projection tomography as a tool for 3D imaging of hydrogels", *Biomed. Opt. Express* 5(10), 3443-3449, 2014.

[2] L. Chen. "Development of optical projection tomography for mesoscopic 3D biomedical imaging", PhD. thesis, photonics group, department of physics , Imperial College, London, 2014.

[3] S. Abbas, "Optical projection tomography as a tool to analyze 3D cell culture of cardiomyocytes", M.Sc.thesis, Tampere University of Technology, Finland, 2015.

[4] A.Trull, J. van der Horst, W. J. Palenstijn , L. J. van Vliet , T. Leeuwen and J. Kalkman, "Point spread function based image reconstruction in optical projection tomography", May, 2017.

[5] J. R. Walls, J. G. Sled, J. Sharpe and R. M. Henkelman ,"Correction of artefacts in optical projection tomography", *Phys. Med. Biol.* 50 (2005) 4645-4665, Sep. 2005.

[6] U.J. Birk, A. Darrell, N. Konstantinides, A. Sarasa-Renedo, and J. Ripoll, "Improved reconstructions and generalized filtered back projection for optical projection tomography", *Applied optics* , Vol. 50, No. 4, Feb. 2011.

[7] C. Raven, "Numerical removal of ring artifacts in microtomography", volume 69, number 8, Aug. 1998.

[8] J.V. Derhorst and J. Kalkman, "Image resolution and deconvolution in optical tomography", *OPtics Express 24460* Vol. 24, No. 21, Oct. 2016.

[9] E. Meijering, "Cell Segmentation: 50 Years Down the Road", *IEEE Signal Processing Magazine*, Vol. 29, No. 5, pp. 140-145, Sep. 2012.

[10] A. Arranz, D. Dong, S. Zhu, M. Rudin, C. Tsatsanis, J. Tian and J. Ripoll ,"Helical optical projection tomography ", *Optics Express 25912* Vol. 21, No. 22, DOI:10.1364, OE.21.025912, Nov. 2013.

[11] J. Sharpe, U. Ahlgren, P.Perry, B. Hill, A. Ross, J. H. Sorensen, R. Baldock and D. Davidson. (2002, Apr.) " Optical Projection Tomography as a Tool for 3D Microscopy and Gene Expression Studies", *Science 296*[on line], DOI: 10.1126, science.1068206 Available: http://classic.sciencemag.org [Feb 4, 2016.]

[12] A.M. Soto, J.T. Koivisto ,J.E. Parraga , J. Silva-Correia,J.M. Oliveria, R.L. Reis , M. Kellomaki, J. Hyttinen and E. Figueiras , "Optical Projection Tomography Technique for Image Texture and Mass Transport Studies in Hydrogels Based on Gellan Gum", *Langmuir.*, 32(20):5173-82, May, 2016.

[13] K. Lee, J. Avondo, H. Morrison, L. Blot, M. Stark, J. Sharpe, A. Bangham and E. Coen, "Visualizing Plant Development and Gene Expression in Three Dimensions Using Optical Projection Tomography", *The Plant Cell*, Vol. 18, 2145-2156, Sep. 2006.

[14] N. Andrews, M-C. Ramel, Kumar, Y. Alexandrov, D.J. Kelly, S.C. Warren , L.Kerry, N. Lockwood, A. Frolov, P. Frankel, L. Bugeon, J. McGinty, M.J. Dallman and P.M.W. French, "Fluorescence lifetime optical projection tomography and FRET applied to visualizing apoptosis in live zebrafish larvae ", *Biomedical Optics Congress*, 2016.

[15] B. Belay, J.T. Koivisto, K. Vuornos , T. Montonen, O. Koskela, M. Lehti-Polojarvi, S. Miettinen, M. Kellomaki , E. Figueiras and J. Hyttinen , "Optical Projection Tomography Imaging of Single cells in 3D Gellan Gum Hydrogel", *IFMBE Proceedings* Vol. 65, 2017.

[16] E. Battenberg and I.Bischofs-Pfeifer,"A System for Automatic Cell Segmentation of Bacterial Microscopy Images", Arkin Laboratory For Dynamical Genomics, Lawrance Berkeley National Laboratory, 2006.

[17] F. Jin, P. Fieguth, L. Winger and E. Jernigan,"Adaptive wiener filter of noisy images and image sequences ", Department of Systems Design Engineering University of Waterloo, Waterloo, Ontario, Canada, N2L 3G1.

[18] V. Strela, "Denoising Via Block Wiener Filtering in Wavelet Domain".

[19] M. Nagu, N.V. Shanker, "Image De-Noising By Using Median Filter and Weiner Filter", *International Journal of Innovative Research in Computer and Communication Engineering* Vol. 2, Issue 9, Sep. 2014.

[20] F. Y. Shih, S.Cheng, "Automatic seeded region growing for color image segmentation", Computer Vision Laboratory, College of Computing Sciences, New Jersey Institute of Technology, Newark, NJ 07102, USA, May, 2005.

[21] G. Lathen, "Segmentation methods for medical image analysis, blood vessels, multiscale filtering and levelset methods", department of science and technology, Linkoping University, SE60174, Sweden, Apr. 2010.

[22] C. Zheng, K. Ahmad, "The segmentation of images of biological cells- A survey of methods and systems", *Image segmentation review Manuscript*, Oct. 2008.

[23] M. Liao , Y.-Q Zhao , X.-H. Li , .-s. Dai, X.-w. Xu, J.-K. Zhang, B.-J. Zou , "Automatic segmentation for cell images based on bottleneck detection and ellipse fitting", *Neurocomputing 173* (2016) 615-622, Aug. 2015.

[24] P.Elayaraja and M.Suganthi, "Survey on medical image segmentation algorithms", *International Journal of Advanced Research in Computer and Communication Engineering* Vol. 3, Issue 11, Nov. 2014.

[25] S.Kamdi, R.K. Krishna, "image segmentation and region growing algorithm", *International Journal of Computer Technology and Electronics Engineering (IJCTEE)* Volume 2, Issue 11.

[26] J. B.T.M. Roerdink and A. Meijster, "The Watershed Transform: Definitions, Algorithms and Parallelization Strategies", *Fundamenta Informaticae 41*,187-228 1 IOS Press, 2001.

[27] T. Atta-Fosu, W.Guo, Dana Jeter, C. M. Mizutani, N. Stopczynski, and R. Sousa-Neves, "3D Clumped Cell Segmentation Using Curvature Based Seeded Watershed", *Journal of imaging*, Nov. 2016.

[28] R. Adams, L.Bischof, "Seeded region growing", *IEEE Trans. Pattern Anal. Machine Intell* 16, 641-647, 1994.

[29] A.A. Malek, W. E. Zarina W. A. Rahman, A. Ibrahim, R. Mahmud, S. S. Yasiran, A. K. Jumaat, "Region and Boundary Segmentation of Microcalcifications using Seed-Based Region Growing and Mathematical Morphology", *International Conference on Mathematics Education Research*, 2010.

[30] S. Kansal, P. Jain, A. Kumar, K. Ghaziabad, "automatic seed selection algorithm for image segmentation using region growing", UP, India, 2015.

[31] B.Shanthi, G. GnanambalIlango, "A Segmentation Algorithm Using Neighbourhoods", Vol.1, No.2, Dec. 2015.

[32] J. T. Koivisto, T. Joki, J.E. Parraga, R. Pääkkönen, Laura Ylä-Outinen, L. Salonen, I. Jönkkäri, M. Peltola, T. O. Ihalainen, S. Narkilahti, "Bioamine-crosslinked gellan gum hydrogel for neural tissue engineering", *Biomedical Materials*, Volume 12, Number 2, Mar. 2017.

[33] R. C.Gonzalez, R. E.Woods, digital image processing , second edition , Pearson printice hall, pearson education interanational, 2002, pp 262-266.

[34] J.R.Parker, "Algorithms for image processing and computer vision", Wiley Publishing, Inc, 1043, crosspoint, Boulevard, 2011.

[35] P. Roberts, "Moving averages, the heart of trend analysis", the London Bullion Market Association.

[36] J. Ollion, J.Cochennec, F. Loll, C. Escude and T. Boudier. (2013) TANGO: "A Generic Tool for High-throughput 3D Image Analysis for Studying Nuclear Organization". *Bioinformatics* 15;29(14):1840-1, Jul. 2013.